




 Cite this: *RSC Adv.*, 2023, 13, 29496

Synthesis of new class of indole acetic acid sulfonate derivatives as ectonucleotidases inhibitors†

 Muhammad Siraj Khan Jadoon,^{ab} Julie Pelletier,^c Jean Sévigny ^{cd}
 and Jamshed Iqbal ^{*abe}

Ectonucleotidases inhibitors (ENPPs, e5'NT (CD73) and *h*-TNAP) are potential therapeutic candidates for the treatment of cancer. Adenosine, the cancer-developing, and growth moiety is the resultant product of these enzymes. The synthesis of small molecules that can increase the acidic and ionizable structure of adenosine 5-monophosphate (AMP) has been used in traditional attempts to inhibit ENPPs, ecto-5'-nucleotidase and *h*-TNAP. In this article, we present a short and interesting method for developing substituted indole acetic acid sulfonate derivatives (**5a–5o**), which are non-nucleotide based small molecules, and investigated their inhibitory potential against recombinant *h*-ENPP1, *h*-ENPP3, *h*-TNAP, *h*-e5'NT and *r*-e5'NT. Their overexpression in the tumor environment leads to high adenosine level that results in tumor development as well as immune evasion. Therefore, selective, and potent inhibitors of these enzymes would be expected to decrease adenosine levels and manage tumor development and progression. Our intended outcome led to the discovery of new potent inhibitors like **5e** (IC₅₀ against *h*-ENPP1 = 0.32 ± 0.01 μM, 58 folds increased with respect to suramin), **5j** (IC₅₀ against *h*-ENPP3 = 0.62 ± 0.003 μM, 21 folds increase with respect to suramin), **5c** (IC₅₀ against *h*-e5'NT = 0.37 ± 0.03 μM, 115 folds increase with respect to sulfamic acid), **5i** (IC₅₀ against *r*-e5'NT = 0.81 ± 0.05 μM, 95 folds increase with respect to sulfamic acid), and **5g** (IC₅₀ against *h*-TNAP = 0.59 ± 0.08 μM, 36 folds increase with respect to Levamisole). Molecular docking studies revealed that inhibitors of these selected target enzymes induced favorable interactions with the key amino acids of the active site, including Lys255, Lys278, Asn277, Gly533, Lys528, Tyr451, Phe257, Tyr340, Gln465, Gln434, Lys437, Glu830, Cys818, Asn499, Arg40, Phe417, Phe500, Asn503, Asn599, Tyr281, Arg397, Asp526, Phe419 and Tyr502. Enzyme kinetic studies revealed that potent compounds such as **5j** and **5e** blocked these ectonucleotidases competitively while compounds **5e** and **5c** presented an un-competitive binding mode. **5g** revealed a non-competitive mode of inhibition.

 Received 25th June 2023
 Accepted 2nd October 2023

DOI: 10.1039/d3ra04266a

rsc.li/rsc-advances

Introduction

The proliferation of tumors is perhaps dependent on immune cell infiltration and the release of inflammatory mediators by these infiltrating immune cells, according to currently available data.¹ Tumors use various immunosuppressive mechanisms

that aid non-responders avert the immune system and modulate the tumor microenvironment and angiogenesis.^{2,3} In order to enhance clinical outcomes, combination treatments that aim to target a variety of immunosuppressive pathways may be necessary for improved cancer treatment.⁴ One way that tumors avoid the immune system is through reducing adenosine-like small molecule signaling chemicals in the tumor microenvironment. Adenosine, has been demonstrated to accumulate in tumors and have potent immunosuppressive effects on a variety of tumor-infiltrating leukocytes (TILs) through the A_{2A}/A_{2B} adenosine receptors.⁵ In fact, elevated levels of ATP, AMP and adenosine in the tumor microenvironment are emerging as important modulators of cancer-related inflammation, supporting tumor development as well as immune evasion.⁶

The members of ectonucleotidases family such as e5'NT (ecto-5'-nucleotidase, CD73), ectonucleotide pyrophosphatases/phosphodiesterases (ENPPs) and human tissue nonspecific alkaline phosphatase (*h*-TNAP) which changes the extracellular

^aDepartment of Pharmacy, COMSATS University Islamabad, Abbottabad Campus, Abbottabad, 22060, Pakistan. E-mail: drjamshed@cuiatd.edu.pk; jamshediqb@googlemail.com

^bCentre for Advanced Drug Research, COMSATS University Islamabad, Abbottabad Campus, Abbottabad, 22060, Pakistan

^cCentre de Recherche du CHU de Québec-Université Laval, Québec G1V 4G2, Canada

^dDépartement de microbiologie-infectiologie et d'immunologie, Faculté de Médecine, Université Laval, Québec G1V 0A6, Canada

^eDepartment of Chemistry, COMSATS University Islamabad, Abbottabad Campus, Abbottabad, 22060, Pakistan

† Electronic supplementary information (ESI) available. See DOI: <https://doi.org/10.1039/d3ra04266a>



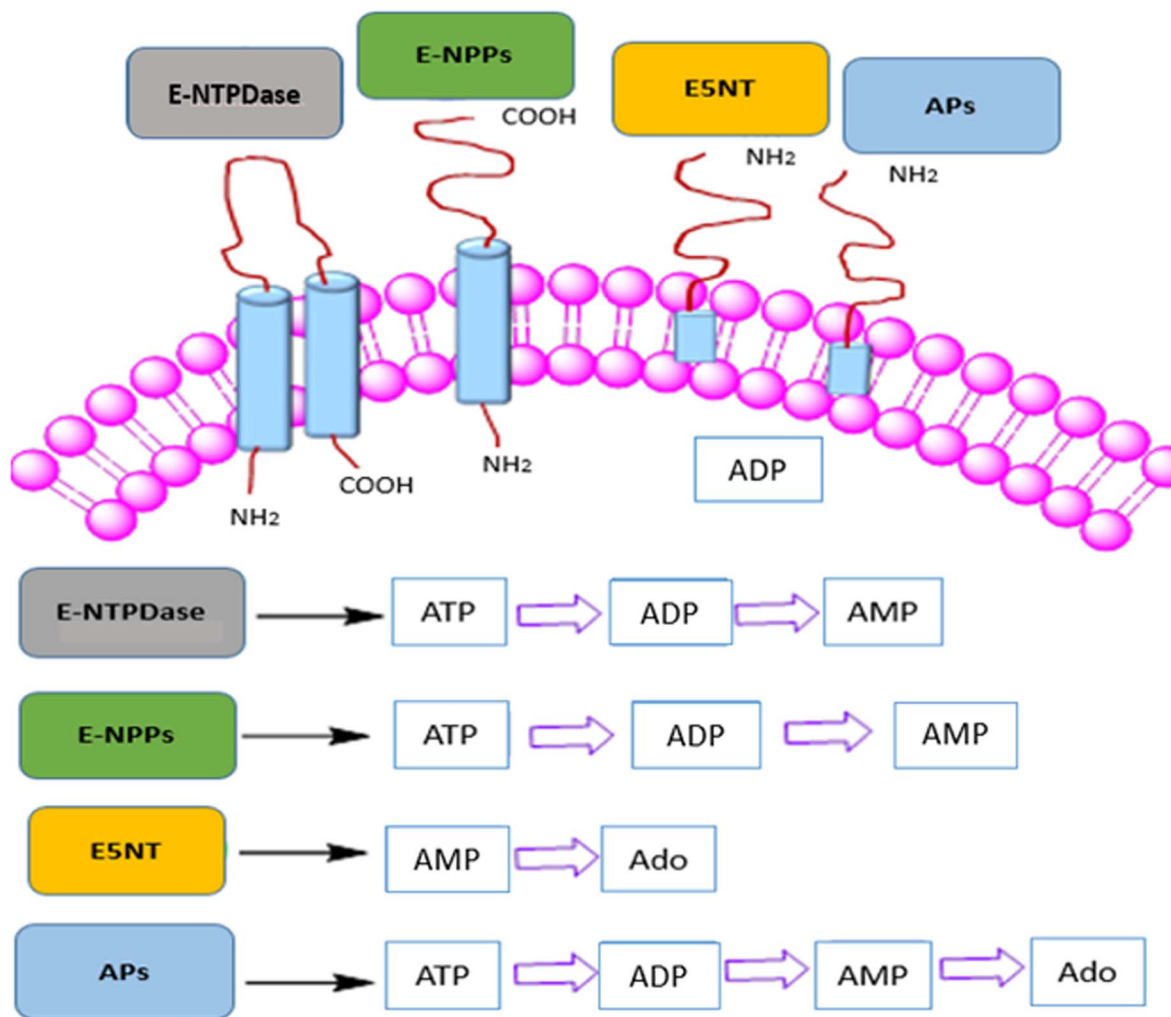


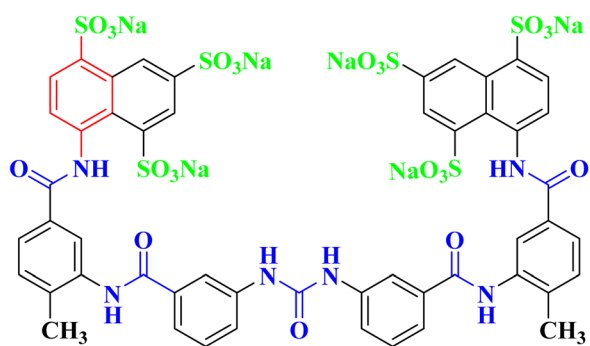
Fig. 1 Ectonucleotidases family presented with catalytic transformation of adenosine triphosphate (ATP) into adenosine monophosphate (AMP) and adenosine (Ado).

level of adenosine triphosphate (ATP) into adenosine monophosphate (AMP) and finally to adenosine (as shown in Fig. 1), that controls the intratumoral synthesis of adenosine.^{7–15} Adenosine, which is produced by the hydrolysis of the ATP and AMP *via* ENPPs, e5'NT and *h*-TNAP, is crucial for many therapeutically essential processes, including anti-inflammatory,^{16–18} vasodilatation, and antidiuretic effects,¹⁹ immunosuppression,^{20,21} and antinociceptive effects.²² Numerous human malignancies have been discovered to overexpressed NPPs, e5'NT and, *h*-TNAP, which is expressed on a variety of cell surfaces including myocardial ischemia, insulin resistance, carcinogenesis and metastasis of tumor cell, and hypermineralization like calcific aortic valve disease.^{21–23} Moreover, a weak clinical prognosis is linked to increased e5'NT expression.^{24–26} It is anticipated that these ectonucleotidases inhibition can reverse adenosine buildup in the tumor microenvironment, including adenosine mediated immunity suppression by obstructing the primary tumor microenvironment-based adenosine synthesis mechanism.^{5,27,28}

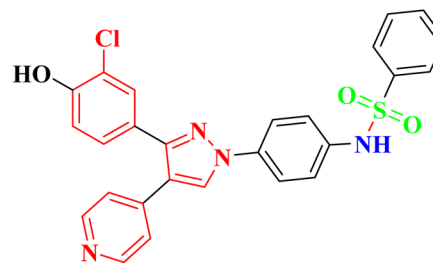
These ectonucleotidases, belong to the metalloprotease family of enzymes. e5'NT has been found to be significantly

expressed by melanoma cells, while levels of e5'NT have been linked to the propensity of these cells to metastasis.^{29,30} Adenosine and e5'NT play roles in immunological responses, including those that involves T cells and B cells,³¹ as well as in the development of tumors.³² e5'NT inhibitors have the potential to be used in illness treatments that aim to lower adenosine levels.^{30,33} Additionally, specific e5'NT inhibitors may be helpful pharmacologically as well as for purposes of diagnosis. ENPPs are present as transmembrane bound glycoproteins and soluble proteins, constituting a family of seven members (NPP1-7).^{34,35} Among these, NPP1-3 are well characterized and *h*-ENPP1 and 3 (membrane bound glycoproteins) have superior nucleotide hydrolyzing activity than NPP2 (soluble protein). *h*-ENPP1 and *h*-ENPP3 are found on the surface of basophil cells, mast cells,³⁶ mucosal and epithelial cell surfaces.³⁷ The overexpression of *h*-ENPP1 suppresses the tyrosine kinase based activity of insulin receptors²³ including human stem cells³⁸ and brain cancer³⁹ whereas *h*-ENPP3 act as diagnostic marker for allergen (IgE) sensitivity^{36,37} and tumor marker.^{21,40} Since both *h*-ENPP1 and *h*-ENPP3 are isozymes that play a role in a number of clinical illnesses, finding biologically active chemicals to change how

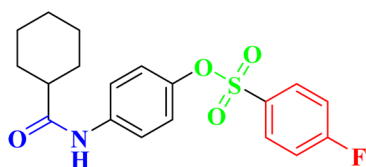


**Suramin**

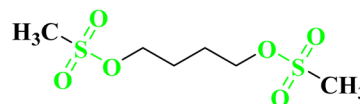
Std. drug for ENPPs

**Pyrazole Sulfonamide derivative**

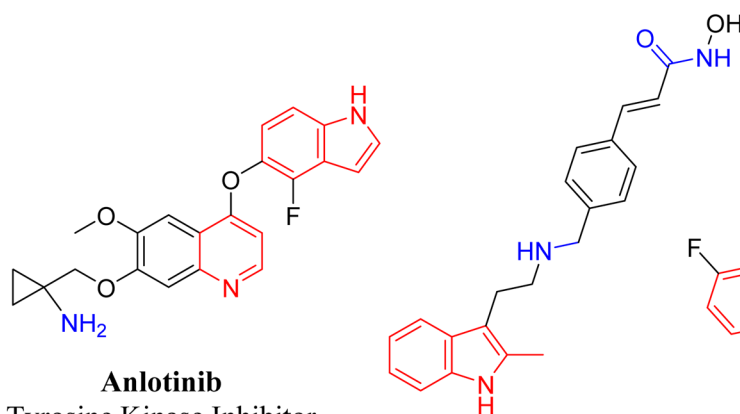
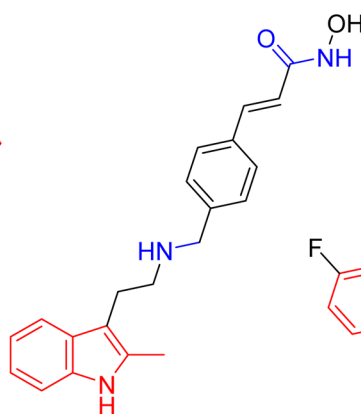
Ectonucleotidase inhibitor

**Cyclohexanecarboxylic acid Sulfonate derivative**

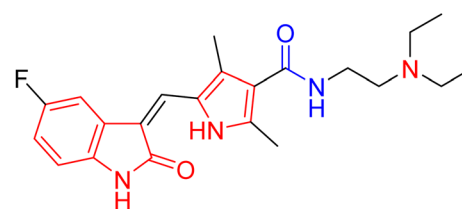
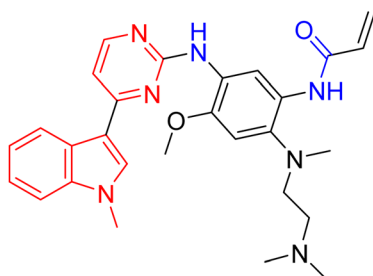
Ectonucleotidase inhibitor

**Busulfan**

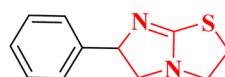
Anticancer drug

**Anlotinib**Tyrosine Kinase Inhibitor
(Non-small Cell Lung Cancer)**Panobinostat**

Multiple Myeloma

**Sunitinib**Receptor Tyrosine Kinase Inhibitor
(Renal cell carcinoma)**Osimertinib**

(EGFR) inhibitor

**Levamisole**

Std. drug for APs

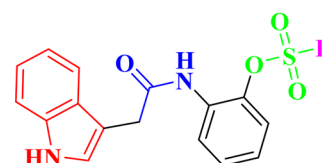
**Current work**

Fig. 2 Molecules from literature, reported for exhibiting ectonucleotidases inhibitory and anticancer activity, having either sulfonate, carboxamide or indole moiety in major nucleus of scaffolds.

they operate has been a popular area of research to discover novel drugs. In case of APs the four different isozymes that make up the tissue-specific and tissue-nonspecific alkaline

phosphatases have been encoded in separate gene loci.⁴¹ Nonspecific alkaline phosphatases are found in the kidney, liver, and bones while tissue-specific APs are further classified into



intestinal, placental, and germ cell alkaline phosphatases.⁴² Numerous diseases, including carcinoma of the breast, behavioral disorders, and severe medical conditions including osteoarthritis, ankyloses, and calcification of the vascular system are brought on by the overproduction of these enzymes.⁴³ Alkaline phosphatase (*h*-TNAP) upregulation and many cancer types are closely related. Most often, cells originating from the breast cancer region exhibit placental APs overexpression. Likewise, to hepatocellular carcinoma, increased saturation of intestine and germ cell APs was observed in the case of choriocarcinoma.⁴⁴ In addition to the biological application already mentioned, *h*-TNAP is crucial for purinergic signaling in a number of malignancies (Fig. 2).

Affirming the role of ENPPs, e5'NT and *h*-TNAP in numerous pathophysiological conditions including cancer, various therapeutic interventions have been employed. By inhibiting these enzymes, the adenosine moiety, one of the causes of cancer development and progression could be limited. One of the most important sources of bioactive molecules is heterocyclic

compounds, which can be produced in a laboratory or derived from natural sources.^{45–47} Because these heterocyclic compounds contain one or more heteroatoms with the potential to donate and accept H-bonds, such as N, O, and S, they can easily attach to a variety of therapeutic targets, producing a wide range of biological effects.⁴⁸ Variety of heterocyclic molecules with ectonucleotidases inhibitory potential either nucleotide or non-nucleotide^{49–54} have been synthesized till date including inhibitors of natural origin to target cancer using different modes.^{55,56} A nucleotide-based ectonucleotidase inhibitor drug, Quemliclstat (AB680), is under phase 1 clinical trials for the treatment of tumors.⁵² One such non-nucleotide class of inhibitors is a variety of sulfonates reported active against the ectonucleotidases with K_i values in low micro-molar ranges.^{57–61} Sulfonates have been reported to be anticancer agents with additional therapeutic potentials. Since 1959, persistent myeloid leukaemia, refractory lymphoma and myeloproliferative ailments have all been treated with busulfan, one of the alkyl sulfonate.⁶² The antiproliferative effects of a number of sulfonate esters were tested on the human breast cancer cell line MCF-7, among these compounds *p*-methoxyphenyl *p*-toluenesulfonate and 3-methoxyphenyl *p*-toluenesulfonate significantly decreased cell viability, with lowest IC_{50} values of 125.9 μ M and 89.8 μ M, respectively.⁶³ Similarly ectonucleotidase inhibitors, pyrazole sulfonate derivatives expressed good activity against (MCF-7) breast cancer cell line, cervical cancer cell line (HeLa), bone marrow cancer cell line (K-562) and brain astrocytoma cell line (1321N1).⁶⁴ In the present study indole acetic acid sulfonate derivatives (5a–5o) were synthesized and investigated for *in vitro* activity against selected ectonucleotidases (ENPPs, e5'NT and *h*-TNAP). The newly synthesized sulfonate derivatives exhibited noticeable inhibitory potential against the investigated enzymes. The inhibitory potential of compounds 5c, 5e, 5g, 5i, and 5j showed IC_{50} values in the sub micromolar range of 0.32 to 0.81 μ M as shown in Fig. 4.

Among the heterocyclic compounds, nitrogen heterocycles, particularly indole, are thought to be among the most

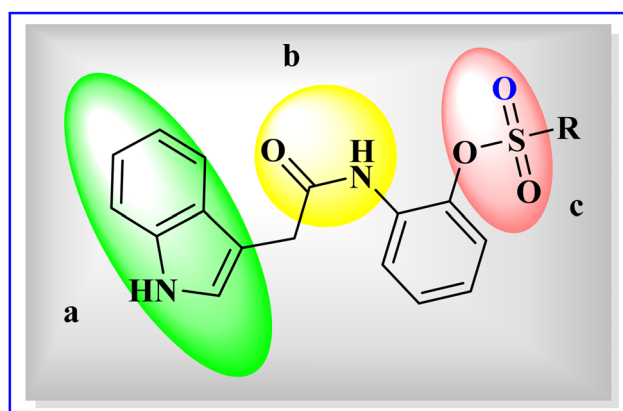


Fig. 3 General structure of indole acetic acid sulfonate derivatives (5a–5o), (a) indole ring, (b) carboxamide group, and (c) sulfonate group.

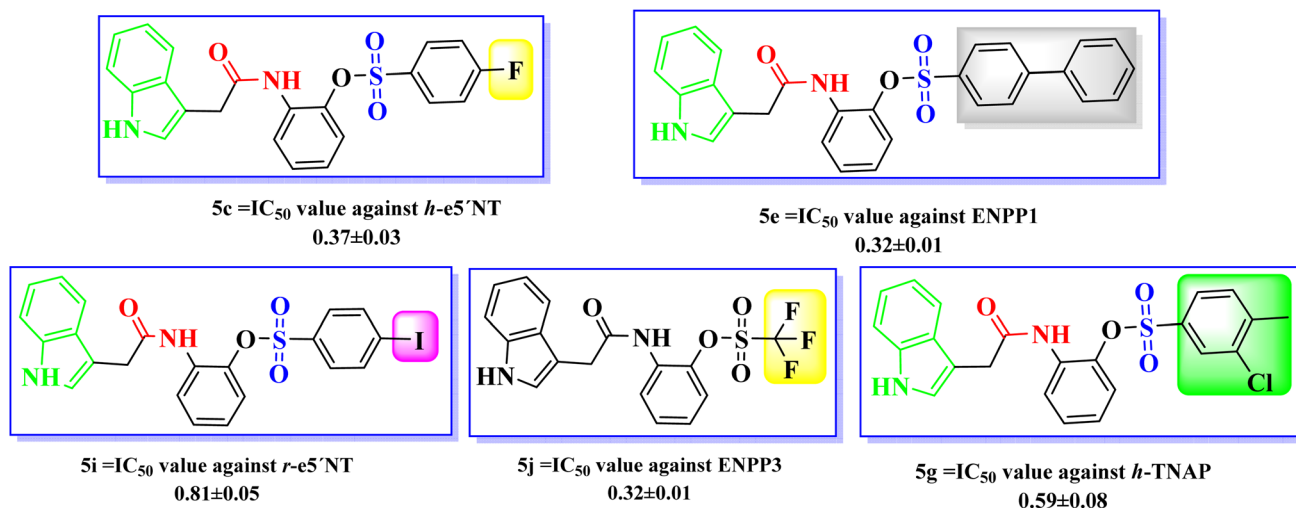


Fig. 4 Most potent compounds among indole acetic acid sulfonate derivatives (5a–5o).



significant nitrogen heterocyclic cores that have attracted significant research in recent years due to its numerous bioactivities.⁶⁵ The indole moiety, which is made up of a combination of aromatic and heterocyclic compounds, serves as a useful framework for the synthesis of new leads.⁶⁶ Various indole based newly synthesized compounds showed remarkable activity against numerous cancers. This is the reason that indole based drugs have been in common practice for the treatment of various cancers since long. Such clinically applied indole-based anticancer medications include panobinostat,⁶⁷ alectinib,⁶⁸ sunitinib,⁶⁹ osimertinib,⁷⁰ anlotinib, and nintedanib.⁷¹ Keeping in consideration, indole based drugs role in cancer treatment *via* different mechanism the newly synthesized compounds with indole, carboxamide and sulfonate substituents are focused to target cancer *via* ectonucleotidases inhibition, involved in the synthesis of adenosine that develop and promotes different cancers.

Our current work expresses indole acetic acid derivatives with sulfonate, carboxamide, and indole moiety unified in newly synthesized molecules important for ectonucleotidases inhibitory activity as shown in Fig. 3. These compounds were found potentially very active against all the targeted enzymes which contribute to the high level of adenosine formation in tumor microenvironment. Exhibition of excellent inhibitory activities by the synthesized indole acetic acid sulfonate derivatives against ENPPs, e5'NT and *h*-TNAP pose their importance as a candidate in tumors management strategies with improved IC₅₀ values than the existing compounds of this class.

Results and discussion

Chemistry

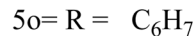
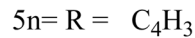
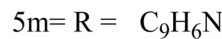
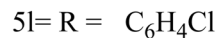
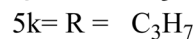
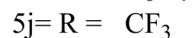
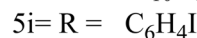
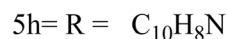
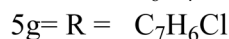
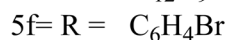
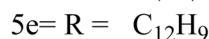
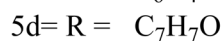
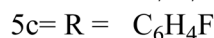
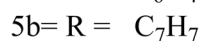
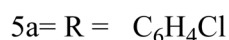
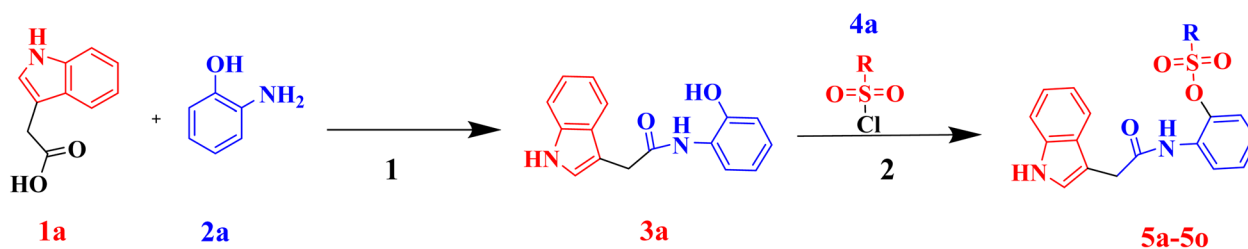
The indole acetic acid sulfonate derivatives (**5a–5o**) were synthesized by facile *in situ* synthesis as shown in Scheme 1. In first step the *N*-(2-hydroxyphenyl)-2-(1*H*-indol-3-yl)acetamide (**3a**) was

synthesized by treating 2-aminophenol (**1a**) with 2-indole acetic acid (**2a**) in the presence of 4-(dimethylamino)pyridine (DMAP) and carbonyldiimidazole (CDI). In the next step the synthesized compound **3a**, was treated with substituted sulfonyl chlorides (**4a**) in the presence of triethylamine (TEA) and acetonitrile as a solvent. The reaction was allowed for 24 hours followed by workup of the reaction resulting in the formation of indole acetic acid sulfonate derivatives (**5a–5o**) in a good to excellent yield.

Physical properties like melting points and color of final products were also determined. Structure elucidation of indole acetic acid sulfonate derivatives (**5a–5o**) was done using FTIR, ¹H NMR, ¹³C NMR and elemental analysis. In FTIR spectra, absorbance band appeared at 3340–3300, 3150–3194 (free and associated –NH), 2900–2990 (–CH), 1600–1685 (C=O) and 1040–1098 (S=O). In ¹H NMR, two characteristic broad singlets were observed in the range of δ 10.50–12.0 ppm, δ 9.5–8.5 ppm for CONH and NH respectively. In ¹³C NMR, indole ring carbons appear in the region of δ 111.39–136.58 ppm, while carbonyl carbon attached to the NH of carboxamide gives a peak at δ 171.61 ppm and that of carbon atoms attached to sulfonyl groups present a peak at δ 132.87 ppm and δ 140.11 ppm. These characteristic peaks confirmed the formation of indole acetic acid sulfonate derivatives. Purity of compounds was determined through elemental analysis that were found to be within 0.4% of the calculated results.

Enzymatic assays

The synthetic compounds' ability to inhibit the hydrolytic activity of the *h*-ENPP1 and *h*-ENPP3 isozymes, *h*-e5'NT and *r*-e5'NT along with *h*-TNAP was assessed. The activity of these selected enzymes was potentially and significantly inhibited by newly developed compounds. The results of the enzymatic investigation of compounds (**5a–5o**) showed highly potent inhibitors with IC₅₀ values ranging from 0.32 to 0.80 μ M as shown in Table 1. The main scaffold features include the presence of an indole moiety, carboxamide and a sulfonate



Scheme 1 Synthesis of indole acetic acid sulfonate derivatives (**5a–5o**).



Table 1 Ectonucleotidases inhibition at 100 μM per well compound concentration, presented as $\text{IC}_{50} \pm \text{SEM}$ (μM) values or inhibition%

Compound codes	R	$\text{IC}_{50} \pm \text{SEM}$ (μM) ^a or inhibition% ^b				
		<i>h</i> -ENPP1	<i>h</i> -ENPP3	<i>h</i> -e5'NT	<i>r</i> -e5'NT	<i>h</i> -TNAP
5a	C ₆ H ₄ Cl	2.07 \pm 0.22	1.66 \pm 0.007	1.19 \pm 0.02	(22.72)%	1.6 \pm 0.11
5b	C ₇ H ₇	1.35 \pm 0.02	1.71 \pm 0.11	13.22 \pm 3.14	(38.52)%	(42.39)%
5c	C ₆ H ₄ F	1.12 \pm 0.12	1.37 \pm 0.05	0.37 \pm 0.03	1.66 \pm 0.04	1.48 \pm 0.02
5d	C ₇ H ₇ O	1.09 \pm 0.01	2.05 \pm 0.25	3.46 \pm 0.12	1.77 \pm 0.12	5.18 \pm 0.46
5e	C ₁₂ H ₉	0.32 \pm 0.01	4.51 \pm 0.38	0.56 \pm 0.016	0.98 \pm 0.02	1.06 \pm 0.03
5f	C ₆ H ₄ Br	1.14 \pm 0.002	1.23 \pm 0.01	0.69 \pm 0.001	1.64 \pm 0.02	6.58 \pm 0.25
5g	C ₇ H ₆ Cl	1.69 \pm 0.05	1.31 \pm 0.11	4.41 \pm 0.19	1.85 \pm 0.11	0.59 \pm 0.08
5h	C ₁₀ H ₈ N	0.91 \pm 0.02	1.02 \pm 0.004	1.17 \pm 0.13	0.91 \pm 0.04	2.86 \pm 0.06
5i	C ₆ H ₄ I	1.07 \pm 0.06	3.26 \pm 0.15	4.85 \pm 0.55	0.81 \pm 0.05	2.27 \pm 0.24
5j	CF ₃	0.59 \pm 0.003	0.62 \pm 0.003	0.89 \pm 0.04	5.12 \pm 0.61	1.68 \pm 0.07
5k	C ₃ H ₇	1.74 \pm 0.05	0.89 \pm 0.04	(37.52)%	(28.65)%	(31.75)%
5l	C ₆ H ₄ Cl	0.85 \pm 0.03	0.77 \pm 0.03	0.43 \pm 0.03	5.67 \pm 0.11	1.69 \pm 0.18
5m	C ₉ H ₆ N	1.36 \pm 0.09	1.22 \pm 0.01	6.53 \pm 0.67	(30.03)%	1.3 \pm 0.38
5n	C ₄ H ₃	(38.03)%	2.55 \pm 0.07	(44.68)%	(46.64)%	(28.88)%
5o	C ₆ H ₇	(28.32)%	2.67 \pm 0.46	3.21 \pm 0.83	4.86 \pm 0.04	3.37 \pm 0.05
Suramin		18.54 \pm 1.14	12.83 \pm 0.23	—	—	—
Sulfamic acid		—	—	42.1 \pm 7.80	77.3 \pm 7.0	—
Levamisole		—	—	—	—	21.38 \pm 4.17

^a Results are presented as an average value of two independent experiments, which were conducted in triplicate (only compounds with more than 50% inhibitory concentration were subjected to evaluate their IC_{50} values). ^b Percentage inhibition at 100 μM per well inhibitor concentration. (Compounds with less than 50% inhibition are present with inhibition% values).

group, whereas R representing aryl or alkyl moieties attached to the main scaffold as shown in Fig. 3.

Structure activity relationships (SARs)

A new class of indole acetic acid sulfonate derivatives were synthesized and evaluated against human *h*-ENPP1, *h*-ENPP3, *h*-e5'NT, *r*-e5'NT and *h*-TNAP *via in vitro* assay. Compounds presented noticeable inhibitory activity against these selected targets. Among all the synthesized compounds 5c, 5e, 5g, 5i, and 5j were found to be more potent against the target enzymes. The pharmacophore structure including indole ring,

carboxamide group and sulfonate group are responsible for the primary inhibitory activity of the indole acetic acid sulfonate derivatives (5a–5o), whereas substitution to the main scaffold resulted in the increase in inhibitory potential of newly synthesized compounds (as shown in Fig. 5). In case of compound 5c, the substitution of fluorine at para position enhanced the activity of the main scaffold with IC_{50} against *h*-e5'NT = 0.37 μM . Electronegative effect of the fluorine resulted in an increased potency by reducing the hydrolytic activity of the enzyme. It was concluded from the *in vitro* results that fluorine substitution adds to the good inhibitory activity for all targeted enzymes ranging IC_{50} between 0.37 to 1.67 μM .

Biphenyl ring substitution to the main scaffold developed 5e and resulted in very good activity that increase the activity by 57 folds against *h*-ENPP1 as compared to standard inhibitor suramin. Similarly, it increased the activity against *h*-ENPP3, *h*-e5'NT, *r*-e5'NT and *h*-TNAP by 3, 75, 79 and 20 folds, respectively. Compound 5g, when substituted with chloro and methyl groups at ortho and para position respectively, resulted in an increase in its inhibitory potential against *h*-TNAP with an IC_{50} value of 0.59 μM . Electronegative effect of chlorine and presence of methyl group impart increase in inhibitory potential of this compound against all target enzymes as concluded from the *in vitro* activity assay. Additionally, the methyl ring contributes to better pharmacokinetic profile of the compound by enhancing its bioavailability and excretion of the drug from the body. Substitution of iodo group in compound 5i at para position of the scaffold resulted in an increase inhibitory potential of the compound against *r*-e5'NT with an IC_{50} value of 0.81 μM contributing 95 folds increase compared to reference standard sulfamic acid. Compound 5j having a substitution of three strong electronegative fluorine groups resulted in increase in *in*

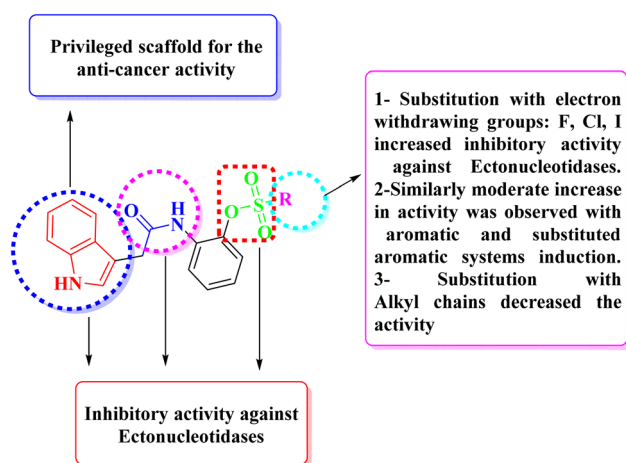


Fig. 5 Illustration of SAR for newly synthesized indole acetic acid sulfonate derivatives (5a–5o) highlighting the role of pharmacophoric core including indole ring, carboxamide, and sulfonate group in main scaffold structure with different substitutions.



Table 2 Binding energy of newly synthesized indole acetic acid sulfonate derivatives against receptor proteins

Ligands	Binding energy (kcal mol ⁻¹)				
	<i>h</i> -ENPP1	<i>h</i> -ENPP3	<i>h</i> -e5'NT	<i>r</i> -e5'NT	<i>h</i> -TNAP
5a	-6.3	-5.9	-6.4	-8.0	-5.1
5b	-6.6	-5.9	-6.4	-8.1	-4.7
5c	-6.6	-5.7	-6.1	-7.7	-5.0
5d	-6.4	-6.1	-6.3	-8.0	-5.1
5e	-8.3	-6.6	-7.6	-8.3	-5.3
5f	-6.7	-6.6	-6.4	-8.0	-5.2
5g	-7.2	-6.3	-6.3	-8.3	-5.0
5h	-7	-6.2	-6.6	-7.7	-5.2
5i	-6.9	-5.9	-5.6	-7.9	-4.9
5j	-5.6	-5.2	-6.0	-6.8	-4.4
5k	-5.9	-5.4	-6.2	-7.1	-4.5
5l	-6.6	-6.1	-6.7	-7.7	-4.9
5m	-6.8	-5.9	-6.7	-8.0	-5.1
5n	-6.5	-5.6	-6.2	-7.5	-4.9
5o	-6.3	-6.1	-6.2	-7.8	-5.1
Ref.	-5.8	-5.4	-11.1	-11.7	-3.5

in vitro determined inhibitory potential of *h*-ENPP3. The incorporation of substitution with strong electronegative group contributed to increase inhibitory potential against target enzymes with IC₅₀ values ranging from 0.59 to 5 μM.

Some compounds showed selectivity and good potency between same enzymes from different species, such as 5a, 5b and 5m expressed good potency and selectivity for *h*-e5'NT as compared to the *r*-e5'NT. Similarly compounds expressed selectivity and high potency between different isozymes such as *h*-ENPP1 and *h*-ENPP3. Substitution of more electronegative chlorine group in compound 5a, phenyl group in compound 5b and quinolone moiety in compound 5m resulted in selectivity of the compounds towards *h*-e5'NT. In a similar way, compound 5n and 5o, which have a thiophene moiety substitution and

a para methyl substitution to the primary scaffold consisting of an indole, a carboxamide, and sulfonate moieties, respectively, were found to be more effective and selective for *h*-ENPP3 between the two *h*-ENPP isozymes (Table 2).

Enzyme kinetic studies for *h*-ENPPs, e5'NT and *h*-TNAP

Enzyme kinetic studies were performed for the most potent inhibitors against *h*-ENPP1, *h*-ENPP3, *h*-e5'NT, *r*-e5'NT and *h*-TNAP. For *h*-ENPP1 and *h*-ENPP3 the potent inhibitors were 5e and 5j, while compound 5c and 5i showed good potential for inhibition of *h*-e5'NT and *r*-e5'NT, whereas, 5g expressed good inhibitory potential against *h*-TNAP. Compound 5j and 5i exhibited competitive mode of inhibition. Inhibitors 5e and 5c presented uncompetitive mode of inhibition as shown in Fig. 6 and 7, whereas, competitive inhibition mode was shown by compound 5g as shown in Fig. 8.

Molecular docking studies analysis

Based upon the binding energy values and results of *in vitro* studies, 3D interactions of potent compounds are visualized in the following figures.

Human ectonucleotide pyrophosphatase/phosphodiesterase 1 (*h*-ENPP1)

Active site amino acids residues involved in the binding interactions of *h*-ENPP1 are;

(1) (Asp218 Lys255 Thr256 Phe257 Asp276 Asn277 Lys278 Ser289 Leu290 Lys291 Lys295 Phe321 Trp322 Pro323 Ser325 Asp326 Lys338 Met339 Tyr340 Tyr371 Glu373 Asp376 Ser377 His380 Ser381 Tyr434 Ile450 Tyr451 Gly452 Pro453 Gln519 Arg527 Lys528 Tyr529 Cys530 Gly531 Ser532 Gly533 Phe534 His535 Po41001 Zn1002).

Protein–ligand 5j interaction showed hydrogen bonding between Lys255 and carbonyl oxygen atom, Lys278 and oxygen

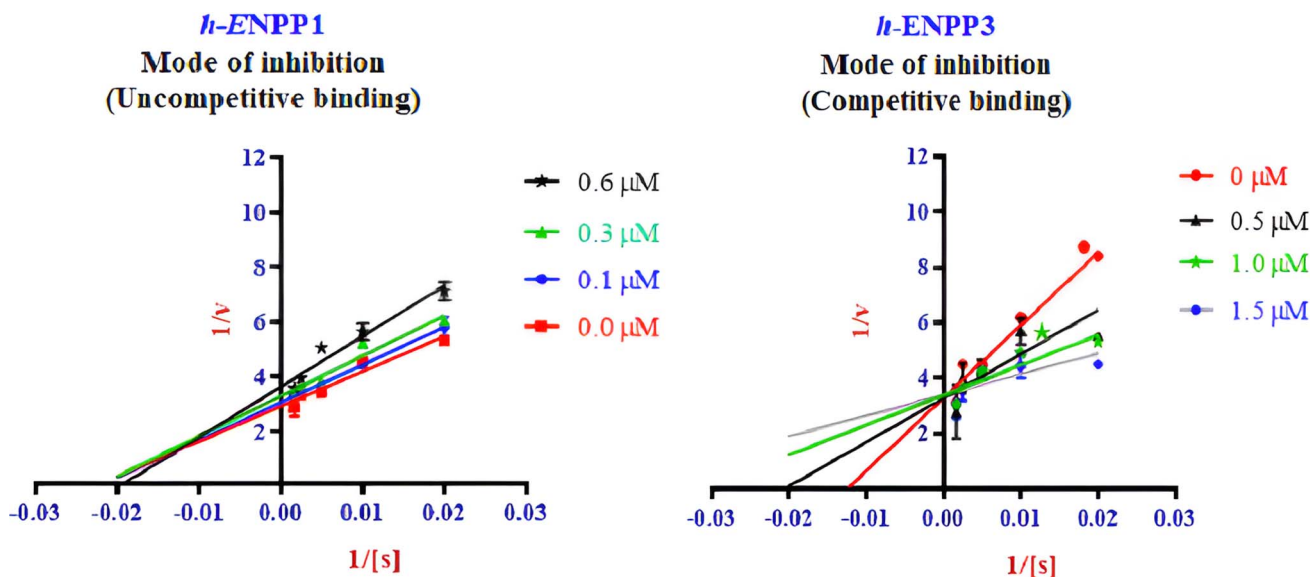


Fig. 6 Illustration of enzyme kinetics for compounds 5e and 5j against human *h*-ENPP1 and *h*-ENPP3, respectively.



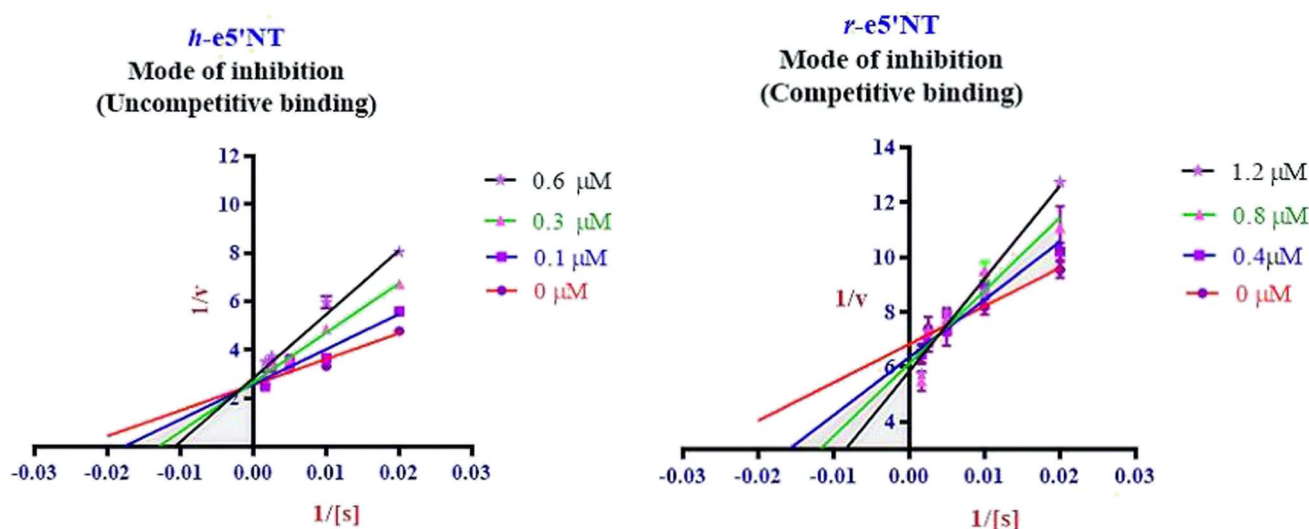


Fig. 7 Illustration of enzyme kinetics for compounds 5c and 5i against *h*-e5'NT and *r*-e5'NT respectively.

atom of sulfonyl group, Asn277 and oxygen atom of sulfonyl group, and hydrogen atom of indole ring and Gly533. One hydrogen bond was also observed between phosphate group and fluorine atom.

In case of ligand 5e amino acid residues Lys528 and Tyr451 are making the hydrogen bonds with the oxygen atom of carbamide group as shown in (Fig. 8). Metal-acceptor interaction was observed between Zn atom and oxygen atom of sulfonyl group. Phe257 and Tyr340 formed π - π stacked and π - π T shaped interaction with the terminal phenyl ring respectively.

Human ectonucleotide pyrophosphatase/phosphodiesterase 3 (*h*-ENPP3)

Amino acids residues in the active site, involved in the active site of *h*-ENPP3 are;

(1): (Lys382 Leu427 Ser428 Cys429 Lys431 Pro432 Asp433 Gln434 His435 Phe436 Lys437 Pro438 Phe462 Val463 Asp464 Gln465 Trp467 Phe489 Val815 Glu816 Ser817 Cys818 Lys822 Trp827 Glu830 Arg831 Ala834).

Binding interaction analysis of 5j revealed that amino acid residue Gln465 made two hydrogen bonds with oxygen atom of sulfonyl group and fluorine atom of trifluoro group (Fig. 9). The hydrogen atom of indole ring formed hydrogen bond with Gln434. In case of 5e, oxygen atom of sulfonyl group made hydrogen bond with Gln465. Gln434 is forming hydrogen bond with hydrogen atom of indole ring. π -cation, π -anion and π -sulphur interactions were observed with amino acid residues Lys437, Glu830 and Cys818 respectively.

Human ecto-5'-nucleotidase (*h*-e5'NT)

Active site amino acids residues involved in the active site of *h*-e5'NT are; (Arg40 Glu46 Asp47 Ser48 Ser49 His243 Ser244 Asn245 Glu257 Tyr281 Phe283 Leu389 Asn390 Gly392 Gly393 Arg395 Leu415 Phe417 Gly418 Gly419 Thr420 Phe421 Asp422 Pro498 Asn499 Phe500 Asn503 Asp506 His518 Asp519 Ser520 Asp524).

In case of compound 5j, amino acid residues Asn499 and Arg40 developed hydrogen bonds with the fluorine atoms of trifluoro group while π - π stacking interaction was found with amino acids Phe417 and Phe500 (Fig. 10). Docking study of protein-ligand interactions of (5c) revealed that amino acid residue Asn503 and Asn599 is involved in hydrogen bonding with both oxygen atoms of sulfonate group. π - π stacking is observed involving indole ring and Phe500 and Phe417 amino acids. π -donor hydrogen bond was observed between terminal ring attached to fluorine and amino acid Tyr281.

Rat ecto-5'-nucleotidase (*r*-e5'NT)

Active site amino acids residues involved in the active site of *r*-e5'NT are; (Gln90 Phe95 Thr96 Lys99 His120 Asp123 Asn124 Ser180 Lys181 Glu182 Phe185 Leu186 Ser187 Asn188 Glu198

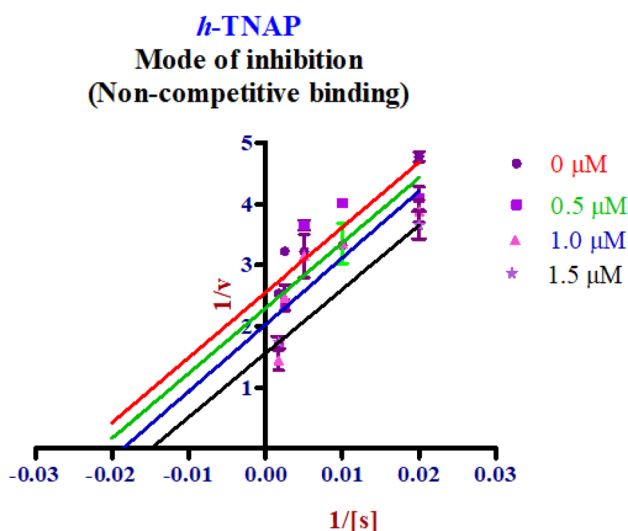


Fig. 8 Enzyme kinetics graphs presenting non-competitive mode of inhibition for compound 5g against *h*-TNAP.



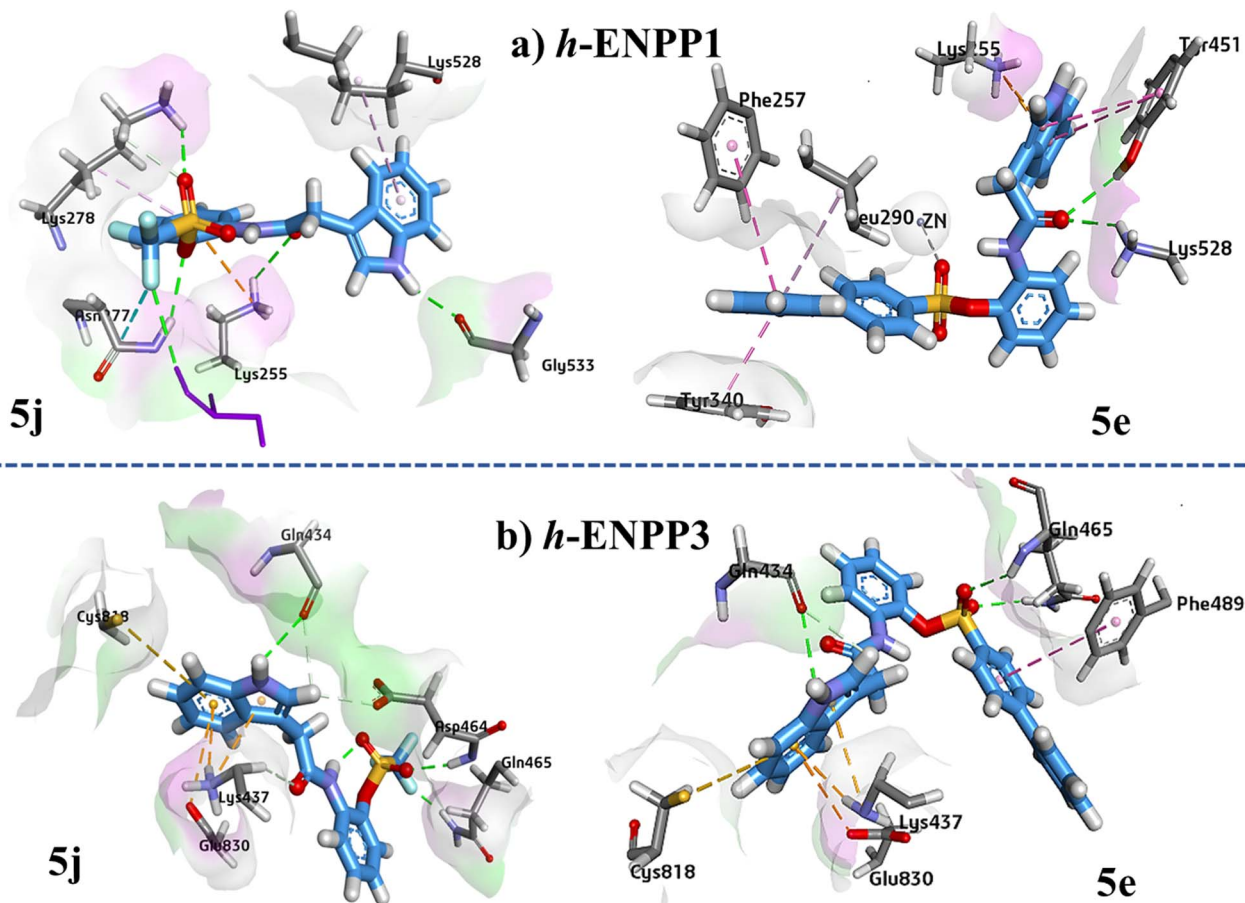


Fig. 9 Illustration of 3D ligand–protein interactions conformations of 5j and 5e against (a) *h*-ENPP1, (b) *h*-ENPP3.

Ser223 Gly224 Phe225 Glu226 Met227 His245 Thr246 Asn247 Arg356 Val391 Asn392 Gly394 Gly395 Arg397 Leu417 Pro418 Phe419 Gly420 Gly421 Thr422 Phe423 Arg443 Gln446 Ser447 Thr448 Gly449 Glu450 Pro500 Ser501 Tyr502 Gly506 Gly507 Asp508 Gly509 Asp526).

Study of binding interaction of 5e showed that pyrrole ring is involved in forming the hydrogen bond with Asp526. While oxygen atom of sulfonyl moiety made hydrogen bond with amino acid residue His120. π -cation and π -anion interaction were observed with Asp508 and Arg397 respectively. Phe419 developed π - π stacking with 5e (as shown in Fig. 10). Synthesized compound 5l showed maximum inhibition potential against *r*-e5'NT. Binding interaction analysis of 5l showed that amino acid residues Asn392 and Arg397 are responsible for hydrogen bonding with the oxygen atoms of carboxamide group. Amino acid Asp526 developed hydrogen bond with the hydrogen atom of pyrrole ring. π - π stacking was observed with amino acid residues Phe419 and Tyr502.

Human tissue nonspecific alkaline phosphatase (*h*-TNAP)

Active site amino acid residues involved in the active site of *h*-TNAP are;

(1) (Ala188 Leu191 Met192 His193 Ile195 Arg196 Asp197 Ile198 Ile201 Met209 Leu235 Trp239 Pro244 Arg245 Tyr246 Lys247 Tyr268 Leu270).

Analysis of indole acetic acid sulfonate derivative 5g presents that amino acid residue Arg196 is responsible for the formation of hydrogen bond with oxygen atom of sulfonyl group while Arg245 developed hydrogen bond with carbonyl oxygen. π -alkyl interactions were observed with amino acid residues Tyr246, Lys247 and His248. In case of 5e, oxygen atom of carboxamide is responsible for hydrogen bonding with Arg245. π -cation interactions were formed with Arg196 (as shown in Fig. 11).

Experimental part

General

All the chemicals and solvents needed for this study were procured from commercial sources and used without additional purification. Analytical grade solvents were used for synthesis while lab grade solvents were employed for purification of newly synthesized compounds. Using the Gallenkamp melting point equipment, the melting point was identified. The thin layer chromatography was carried out using aluminium plates coated with silica gel (0.20 mm, 60 Å), while the spots were detected using a UV absorbance lamp 254–366 nm. For ^1H NMR and ^{13}C NMR Bruker Avance III HD (400 MHz spectrometer) was employed. The multiplicities observed were given as s for singlet, d for doublet, t for triplet, and q for quintet. The



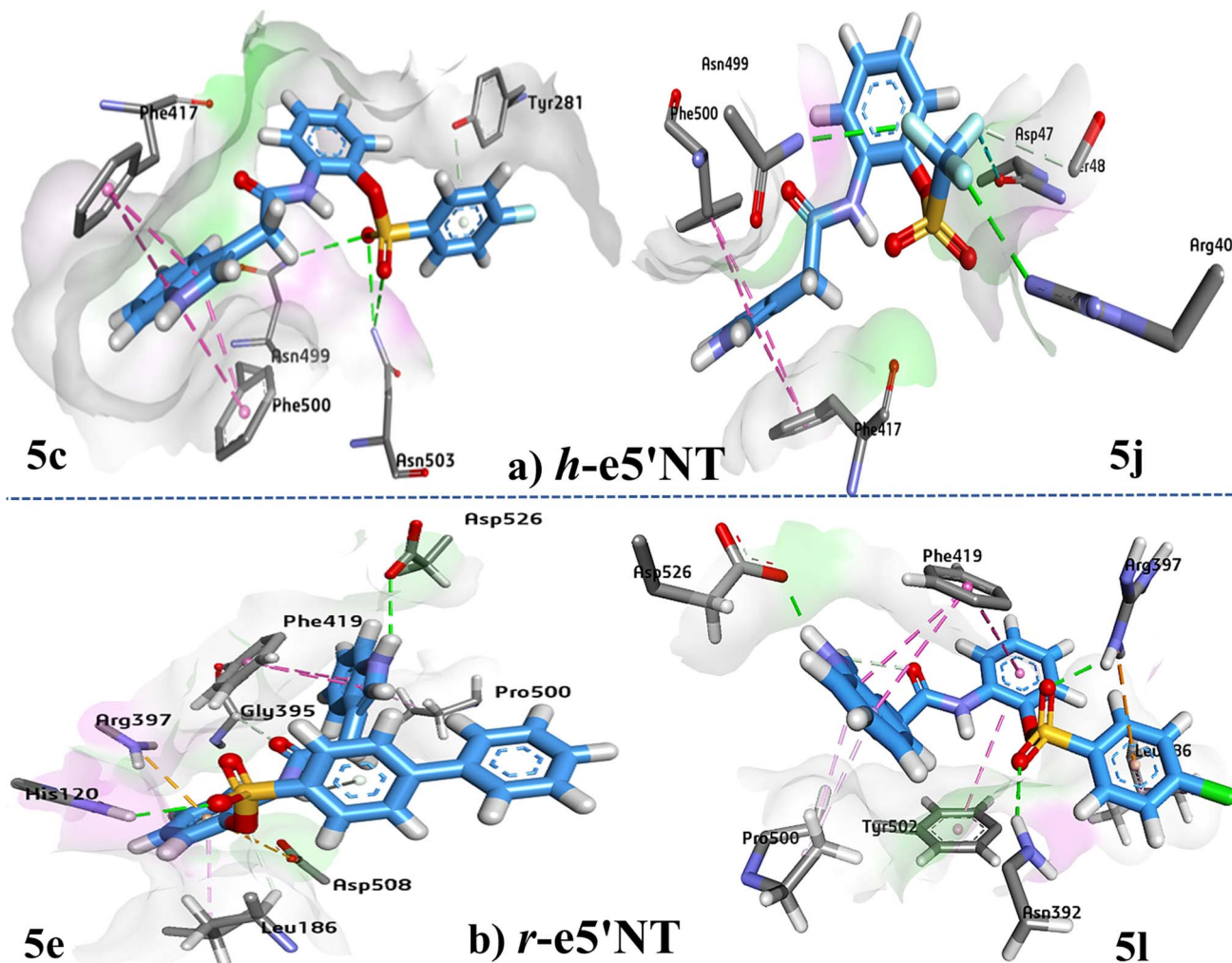


Fig. 10 Presentation of 3D binding modes of inhibitors, 5c and 5j against (a) *h*-e5'NT residues and 5e and 5l against (b) *r*-e5'NT residues.

coupling constant (J) was estimated in Hz. Elemental analysis of the test compounds was carried out using LECO 630-200-200 TruSpec CHNS microanalyzer.

General procedure for the synthesis (5a–5o)

Procedure for the synthesis of *N*-(2-hydroxyphenyl)-2-(1*H*-indol-3-yl)acetamide (3a). In order to synthesize compound 3a,

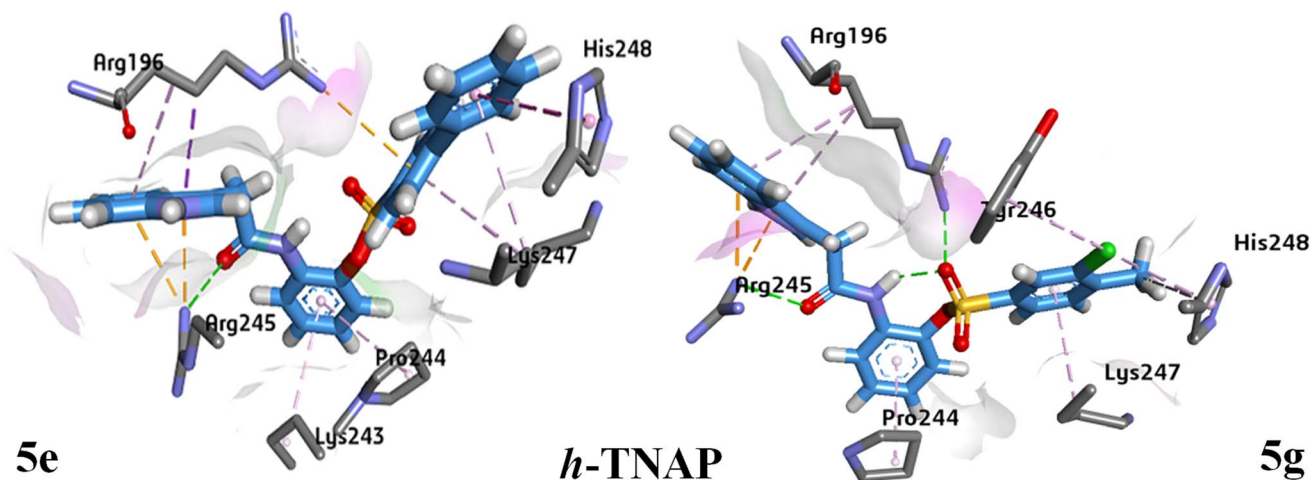


Fig. 11 3D ligand–protein interactions docked conformations presentation for compound 5e and 5g against *h*-TNAP active pocket.



2-indole acetic acid (**1a**) (3.85 mmol; 0.420 g) was combined with 2-aminophenol (**2a**) (2.57 mmol; 0.450 g) incorporating 4-(dimethylamino)pyridine (DMAP) (3.62 mmol; 0.500 g) and carbonyldiimidazole (CDI) (3.62 mmol; 0.500 g) to the reactants while they were being stirred at 80 °C. The reaction mixture was allowed to stir for a further 24 hours at 80 °C. The filtrate was dried, the remaining material was dissolved in ethyl acetate (40 mL) and 5% HCl (30 mL) was used for extraction from the filtrate. After separating the organic layer, a saline solution (50 mL) was used to wash it thrice, the resulted organic layer was collected separately. Using anhydrous sodium sulphate (Na₂SO₄), the separated organic layer was dried of any remaining water molecules before being filtered. The organic solvent was dried off by evaporation, and the resulting compound was employed in the next step.

Synthesis of indole acetic acid sulfonate derivatives (5a–5o).

The desired indole acetic acid sulfonate derivatives (**5a–5o**) were synthesized by reacting **3a** (0.375 mmol; 0.100 g) with different benzene sulfonyl chloride derivatives (**4a**) (0.985 mmol). Triethylamine (TEA) (2.10 mmol) was added dropwise to the reaction mixture at 0 °C and the reactions were completed in acetonitrile (15 mL) as a solvent. Each reaction mixture was thoroughly stirred at 40 °C temperature and quenched three times with equal parts of water and ethyl acetate (30 mL each). The organic layer was dried on a rotary evaporator with anhydrous Na₂SO₄, then washed twice with a saline solution (30 mL), filtered, and dried a third time.

2-(2-(1*H*-indol-3-yl)acetamido)phenyl 2-chlorobenzenesulfonate (5a). Yield: 84.56%, $R_f = 0.4$, (*n*-hexane/ethyl acetate = 1 : 4), colour: off-white solid, mp: 181–183 °C, FT-IR ($\bar{\nu}$, cm⁻¹): 3404 (N–H, stretching), 2958 (C–H, stretching), 1613 (C=O, stretching), 1085 (S=O, stretching); ¹H NMR (400 MHz, DMSO, $\delta =$ ppm): 10.98 (s, 1H), 9.44 (s, 1H), 7.75 (d, $J = 8.1$ Hz, 1H), 7.64 (d, $J = 8.3$ Hz, 2H), 7.56 (d, $J = 8.0$ Hz, 1H), 7.50 (d, $J = 8.3$ Hz, 2H), 7.37 (d, $J = 8.1$ Hz, 1H), 7.25 (q, $J = 8.0$ Hz, 3H), 7.11 (m, 2H), 6.99 (t, $J = 7.5$ Hz, 1H), 3.60 (s, 2H). ¹³C NMR (101 MHz, DMSO, $\delta =$ ppm): 169.90, 140.14, 136.55, 133.84, 133.12, 131.42, 130.45, 129.87, 128.13, 127.71, 125.25, 124.70, 124.52, 123.25, 121.54, 119.22, 118.93, 111.86, 108.57, 33.38. Anal. calcd. for C₂₂H₁₇ClN₂O₄S: C, 59.87; H, 3.89; N, 6.35; S, 7.27%. Found: C, 59.87; H, 3.88; N, 6.38; S, 7.34%.

2-(2-(1*H*-indol-3-yl)acetamido)phenyl phenylmethanesulfonate (5b). Yield: 77.33%, $R_f = 0.5$, (*n*-hexane/ethyl acetate = 1 : 4), colour: off-white solid, mp: 134–137 °C, FT-IR ($\bar{\nu}$, cm⁻¹): 3172 (N–H, stretching), 2931 (C–H, stretching), 1613 (C=O, stretching), 1085 (S=O, stretching); ¹H NMR (400 MHz, DMSO, $\delta =$ ppm): 10.99 (s, 1H), 9.36 (s, 1H), 7.91 (d, $J = 8.1$ Hz, 1H), 7.60 (d, $J = 7.9$ Hz, 1H), 7.39 (m, 3H), 7.39–7.25 (m, 5H), 7.22 (dd, $J = 8.2, 1.7$ Hz, 1H), 7.20–7.11 (m, 1H), 7.05 (t, $J = 7.5$ Hz, 1H), 6.97 (t, $J = 7.4$ Hz, 1H), 4.66 (s, 2H), 3.82 (s, 2H). ¹³C NMR (101 MHz, DMSO, $\delta =$ ppm): 170.44, 136.60, 131.59, 131.50, 129.38, 129.10, 127.96, 127.73, 127.61, 125.55, 124.93, 124.80, 123.06, 121.57, 119.07, 119.01, 111.90, 108.40, 56.52, 33.76. Anal. calcd. for C₂₃H₂₀N₂O₄S: C, 65.70; H, 4.79; N, 6.66; S, 7.62%. Found: C, 65.75; H, 4.73; N, 6.58; S, 7.60%.

2-(2-(1*H*-indol-3-yl)acetamido)phenyl 4-fluorobenzenesulfonate (5c). Yield: 73.84%, $R_f = 0.4$, (*n*-hexane/ethyl acetate = 1 :

4), colour: white solid, mp: 161–163 °C, FT-IR ($\bar{\nu}$, cm⁻¹): 3453 (N–H, stretching), 2937 (C–H, stretching), 1608 (C=O, stretching), 1092 (S=O, stretching); ¹H NMR (400 MHz, DMSO, $\delta =$ ppm): 10.98 (s, 1H), 9.42 (s, 1H), 7.83 (d, $J = 8.1$ Hz, 2H), 7.76 (d, $J = 8.0$ Hz, 1H), 7.57 (d, $J = 7.8$ Hz, 1H), 7.37 (m, 3H), 7.29–7.20 (m, 3H), 7.11 (m, 2H), 7.00 (t, $J = 7.4$ Hz, 1H), 3.59 (s, 2H). ¹³C NMR (101 MHz, DMSO, $\delta =$ ppm): 169.89, 140.14, 138.94, 136.56, 134.21, 131.43, 129.91, 128.09, 127.72, 125.22, 124.65, 124.51, 123.22, 121.54, 119.24, 118.95, 111.86, 108.60, 104.88, 33.41. Anal. calcd. for C₂₂H₁₇FN₂O₄S: C, 62.26; H, 4.04; N, 6.60; S, 7.55%. Found: C, 62.25; H, 4.13; N, 6.68; S, 7.62%.

2-(2-(1*H*-indol-3-yl)acetamido)phenyl 4-methoxybenzenesulfonate (5d). Yield: 79.08%, $R_f = 0.4$, (*n*-hexane/ethyl acetate = 1 : 4), colour: white to off-white solid, mp: 200–203 °C, FT-IR ($\bar{\nu}$, cm⁻¹): 3438 (N–H, stretching), 2963 (C–H, stretching), 1655 (C=O, stretching), 1071 (S=O, stretching); ¹H NMR (400 MHz, DMSO, $\delta =$ ppm): 11.01 (s, 1H), 9.32 (s, 1H), 7.80 (dd, $J = 8.0, 1.6$ Hz, 1H), 7.55 (t, $J = 9.0$ Hz, 3H), 7.38 (d, $J = 8.1$ Hz, 1H), 7.30 (d, $J = 2.4$ Hz, 1H), 7.22 (m, 2H), 7.10 (m, 2H), 7.00 (t, $J = 7.4$ Hz, 1H), 6.93–6.85 (m, 2H), 3.74 (s, 3H), 3.66 (s, 2H). ¹³C NMR (101 MHz, DMSO, $\delta =$ ppm): 169.93, 164.45, 136.58, 131.53, 131.04, 127.80, 127.74, 125.69, 124.92, 124.62, 124.11, 123.05, 121.56, 119.22, 118.93, 115.10, 111.86, 108.59, 56.32, 33.55. Anal. calcd. for C₂₃H₂₀N₂O₅S: C, 63.29; H, 4.62; N, 6.42; S, 7.35%. Found: C, 63.22; H, 4.55; N, 6.38; S, 7.29%.

2-(2-(1*H*-indol-3-yl)acetamido)phenyl [1,1'-biphenyl]-4-sulfonate (5e). Yield: 80.50%, $R_f = 0.35$, (*n*-hexane/ethyl acetate = 1 : 4), colour: off-white solid, mp: 193–195 °C, FT-IR ($\bar{\nu}$, cm⁻¹): 3395 (N–H, stretching), 2954 (C–H, stretching), 1601 (C=O, stretching), 1076 (S=O, stretching); ¹H NMR (400 MHz, DMSO, $\delta =$ ppm): 10.99 (d, $J = 2.5$ Hz, 1H), 9.44 (s, 1H), 7.77 (dd, $J = 8.2, 1.7$ Hz, 1H), 7.70 (d, $J = 8.6$ Hz, 2H), 7.66 (d, $J = 8.6$ Hz, 2H), 7.62–7.40 (m, 6H), 7.40–7.29 (m, 2H), 7.28–7.19 (m, 2H), 7.20–7.04 (m, 2H), 6.96 (ddd, $J = 7.9, 7.0, 1.0$ Hz, 1H), 3.62 (s, 2H). ¹³C NMR (101 MHz, DMSO, $\delta =$ ppm): 169.86, 146.65, 140.12, 136.56, 133.16, 131.49, 129.60, 129.43, 129.27, 127.96, 127.92, 127.74, 127.65, 125.09, 124.54, 124.45, 123.21, 121.55, 119.25, 118.92, 111.87, 108.61, 33.44. Anal. calcd. for C₂₈H₂₂N₂O₄S: C, 69.69; H, 4.60; N, 5.81; S, 6.64%. Found: C, 69.73; H, 4.64; N, 5.78; S, 6.56%.

2-(2-(1*H*-indol-3-yl)acetamido)phenyl 4-bromobenzenesulfonate (5f). Yield: 75.89%, $R_f = 0.4$, (*n*-hexane/ethyl acetate = 1 : 4), colour: off-white solid, mp: 183–186 °C, FT-IR ($\bar{\nu}$, cm⁻¹): 3449 (N–H, stretching), 2963 (C–H, stretching), 1613 (C=O, stretching), 1085 (S=O, stretching); ¹H NMR (400 MHz, DMSO, $\delta =$ ppm): 10.98 (s, 1H), 9.43 (s, 1H), 7.75 (d, $J = 8.5$ Hz, 1H), 7.65 (d, $J = 8.5$ Hz, 2H), 7.59–7.52 (m, 3H), 7.37 (d, $J = 8.4$ Hz, 1H), 7.25 (d, $J = 8.6$ Hz, 3H), 7.11 (m, 2H), 7.01 (d, $J = 7.8$ Hz, 1H), 3.59 (s, 2H). ¹³C NMR (101 MHz, DMSO, $\delta =$ ppm): 169.90, 140.14, 136.55, 133.84, 133.12, 131.42, 130.45, 129.87, 128.13, 127.71, 125.25, 124.70, 124.52, 123.25, 121.54, 119.22, 118.93, 111.86, 108.57, 33.38. Anal. calcd. for C₂₂H₁₇BrN₂O₄S: C, 54.44; H, 3.53; N, 5.77; S, 6.61%. Found: C, 54.73; H, 4.64; N, 5.78; S, 6.56%.

2-(2-(1*H*-indol-3-yl)acetamido)phenyl 3-chloro-4-methylbenzenesulfonate (5g). Yield: 70.15%, $R_f = 0.4$, (*n*-hexane/ethyl acetate = 1 : 4), colour: off-white solid, mp: 115–



117 °C, FT-IR ($\bar{\nu}$, cm^{-1}): 3438 (N–H, stretching), 2948 (C–H, stretching), 1688 (C=O, stretching), 1086 (S=O, stretching); ^1H NMR (400 MHz, DMSO, δ = ppm): 10.95 (s, 1H), 9.47 (s, 1H), 7.82–7.73 (m, 2H), 7.53 (dd, J = 8.1, 1.7 Hz, 2H), 7.42 (d, J = 8.1 Hz, 1H), 7.36 (d, J = 8.1 Hz, 1H), 7.32–7.21 (m, 3H), 7.15 (td, J = 7.8, 1.7 Hz, 1H), 7.08 (m, 1H), 6.98 (m, 1H), 3.58 (s, 2H), 2.35 (s, 3H). ^{13}C NMR (101 MHz, DMSO, δ = ppm): 169.93, 144.17, 140.15, 136.55, 134.67, 133.76, 132.69, 131.46, 128.58, 128.13, 127.70, 127.25, 125.23, 124.42, 123.40, 121.49, 119.15, 118.86, 111.83, 108.58, 33.30, 20.36. Anal. calcd. for $\text{C}_{23}\text{H}_{19}\text{ClN}_2\text{O}_4\text{S}$: C, 60.72; H, 4.21; N, 6.16; S, 7.05%. Found: C, 60.66; H, 4.17; N, 6.05; S, 7.13%.

2-(2-(1H-indol-3-yl)acetamido)phenyl 1-aminonaphthalene-2-sulfonate (5h). Yield: 85.84%, R_f = 0.5, (*n*-hexane/ethyl acetate = 1 : 4), colour: white to off-white solid, mp: 116–118 °C, FT-IR ($\bar{\nu}$, cm^{-1}): 3438 (N–H, stretching), 2927 (C–H, stretching), 1618 (C=O, stretching), 1081 (S=O, stretching); ^1H NMR (400 MHz, DMSO, δ = ppm): 10.93 (s, 1H), 9.40 (s, 1H), 8.68 (dd, J = 8.6, 1.1 Hz, 1H), 8.42 (d, J = 8.2 Hz, 1H), 8.20 (dd, J = 8.3, 1.4 Hz, 1H), 8.10 (dd, J = 7.5, 1.2 Hz, 1H), 7.83 (m, 1H), 7.75 (m, 1H), 7.72–7.62 (m, 2H), 7.49 (d, J = 7.9 Hz, 1H), 7.38–7.31 (m, 1H), 7.24–7.15 (m, 2H), 7.11–6.92 (m, 4H), 6.88 (dd, J = 8.2, 1.5 Hz, 1H), 3.37 (s, 2H). ^{13}C NMR (101 MHz, DMSO, δ = ppm): 169.96, 141.04, 136.98, 136.54, 134.29, 131.79, 130.55, 129.88, 129.71, 128.02, 127.84, 127.65, 125.10, 124.68, 124.46, 122.40, 121.46, 119.08, 118.85, 111.79, 108.47, 33.08. Anal. calcd. for $\text{C}_{26}\text{H}_{21}\text{N}_3\text{O}_4\text{S}$: C, 66.23; H, 4.49; N, 8.91; S, 6.80%. Found: C, 66.16; H, 4.57; N, 8.79; S, 6.76%.

2-(2-(1H-indol-3-yl)acetamido)phenyl 4-iodobenzenesulfonate (5i). Yield: 79.54%, R_f = 0.4, (*n*-hexane/ethyl acetate = 1 : 4), colour: white to off-white solid, mp: 169–172 °C, FT-IR ($\bar{\nu}$, cm^{-1}): 3282 (N–H, stretching), 2947 (C–H, stretching), 1613 (C=O, stretching), 1097 (S=O, stretching); ^1H NMR (400 MHz, DMSO, δ = ppm): 10.98 (s, 1H), 9.42 (s, 1H), 7.83 (d, J = 8.1 Hz, 2H), 7.76 (d, J = 8.0 Hz, 1H), 7.57 (d, J = 7.8 Hz, 1H), 7.37 (dd, J = 8.1, 3.4 Hz, 3H), 7.29–7.20 (m, 3H), 7.11 (dt, J = 15.3, 7.8 Hz, 2H), 7.00 (t, J = 7.4 Hz, 1H), 3.59 (s, 2H). ^{13}C NMR (101 MHz, DMSO, δ = ppm): 169.89, 140.14, 138.94, 136.56, 134.21, 131.43, 129.91, 128.09, 127.72, 125.22, 124.65, 124.51, 123.22, 121.54, 119.24, 118.95, 111.86, 108.60, 104.88, 33.41. Anal. calcd. for $\text{C}_{22}\text{H}_{17}\text{IN}_2\text{O}_4\text{S}$: C, 49.64; H, 3.22; N, 5.26; S, 6.02%. Found: C, 49.76; H, 3.31; N, 5.29; S, 6.11%.

2-(2-(1H-indol-3-yl)acetamido)phenyl trifluoromethanesulfonate (5j). Yield: 84.47%, R_f = 0.4, (*n*-hexane/ethyl acetate = 1 : 4), colour: off-white solid, mp: 114–116 °C, FT-IR ($\bar{\nu}$, cm^{-1}): 3407 (N–H, stretching), 2922 (C–H, stretching), 1618 (C=O, stretching), 1066 (S=O, stretching); ^1H NMR (400 MHz, DMSO, δ = ppm): 10.93 (s, 1H), 10.13 (s, 1H), 7.65–7.54 (m, 2H), 7.53–7.39 (m, 2H), 7.38–7.29 (m, 2H), 7.26 (d, J = 2.4 Hz, 1H), 7.07 (m, 1H), 6.98 (m, 1H), 3.77 (s, 2H). ^{13}C NMR (101 MHz, DMSO, δ = ppm): 170.38, 143.06, 136.55, 131.08, 129.49, 127.75, 127.60, 127.10, 124.53, 122.52, 121.44, 119.04, 118.83, 111.78, 108.32, 32.99. Anal. calcd. for $\text{C}_{17}\text{H}_{13}\text{F}_3\text{N}_2\text{O}_4\text{S}$: C, 51.26; H, 3.29; N, 7.03; S, 8.05%. Found: C, 51.22; H, 3.35; N, 7.08; S, 8.14%.

2-(2-(1H-indol-3-yl)acetamido)phenyl propane-2-sulfonate (5k). Yield: 80.95%, R_f = 0.3, (*n*-hexane/ethyl acetate = 1 : 4),

colour: off-white solid, mp: 139–141 °C, FT-IR ($\bar{\nu}$, cm^{-1}): 3412 (N–H, stretching), 2958 (C–H, stretching), 1605 (C=O, stretching), 1076 (S=O, stretching); ^1H NMR (400 MHz, DMSO, δ = ppm): 11.01 (s, 1H), 9.29 (s, 1H), 7.88–7.81 (m, 1H), 7.58 (d, J = 7.9 Hz, 1H), 7.37 (d, J = 8.1 Hz, 1H), 7.34–7.25 (m, 3H), 7.22–7.14 (m, 1H), 7.13–7.04 (m, 1H), 6.99 (t, J = 7.4 Hz, 1H), 3.80 (s, 2H), 1.21 (d, J = 6.8 Hz, 6H). ^{13}C NMR (101 MHz, DMSO, δ = ppm): 170.28, 140.52, 136.63, 131.26, 127.58, 127.51, 125.68, 125.23, 124.92, 123.02, 121.60, 119.05, 119.02, 111.88, 108.25, 53.26, 33.81, 16.56. Anal. calcd. for $\text{C}_{19}\text{H}_{20}\text{N}_2\text{O}_4\text{S}$: C, 61.27; H, 5.41; N, 7.52; S, 8.61%. Found: C, 61.19; H, 5.36; N, 7.43; S, 8.73%.

2-(2-(1H-indol-3-yl)acetamido)phenyl 4-chlorobenzenesulfonate (5l). Yield: 87.96%, R_f = 0.5, (*n*-hexane/ethyl acetate = 1 : 4), colour: off-white solid, mp: 186–188 °C, FT-IR ($\bar{\nu}$, cm^{-1}): 3376 (N–H, stretching), 2948 (C–H, stretching), 1598 (C=O, stretching), 1071 (S=O, stretching); ^1H NMR (400 MHz, DMSO, δ = ppm): 10.98 (s, 1H), 9.44 (s, 1H), 7.75 (d, J = 8.1 Hz, 1H), 7.64 (d, J = 8.3 Hz, 2H), 7.56 (d, J = 8.0 Hz, 1H), 7.50 (d, J = 8.3 Hz, 2H), 7.37 (d, J = 8.1 Hz, 1H), 7.25 (q, J = 8.0 Hz, 3H), 7.11 (m, 2H), 6.99 (t, J = 7.5 Hz, 1H), 3.60 (s, 2H). ^{13}C NMR (101 MHz, DMSO, δ = ppm): 169.91, 140.63, 140.15, 136.55, 133.39, 131.43, 130.50, 130.16, 128.14, 127.72, 125.26, 124.70, 124.53, 123.25, 121.54, 119.21, 118.92, 111.86, 108.56, 33.37. Anal. calcd. for $\text{C}_{22}\text{H}_{17}\text{ClN}_2\text{O}_4\text{S}$: C, 59.93; H, 3.89; N, 6.35; S, 7.27%. Found: C, 61.01; H, 3.86; N, 6.39; S, 7.25%.

Synthesis of 2-(2-(1H-indol-3-yl)acetamido)phenyl quinoline-8-sulfonate (5m). Yield: 75.37%, R_f = 0.4, (*n*-hexane/ethyl acetate = 1 : 4), colour: off-white solid, mp: 178–180 °C, FT-IR ($\bar{\nu}$, cm^{-1}): 3428 (N–H, stretching), 2922 (C–H, stretching), 1613 (C=O, stretching), 1073 (S=O, stretching); ^1H NMR (400 MHz, DMSO, δ = ppm): 10.93 (s, 1H), 9.53 (s, 1H), 9.19 (dd, J = 4.3, 1.7 Hz, 1H), 8.65 (dd, J = 8.4, 1.8 Hz, 1H), 8.49 (m, 2H), 8.05–7.98 (m, 1H), 7.84 (t, J = 7.8 Hz, 1H), 7.77 (dd, J = 8.3, 4.3 Hz, 1H), 7.48 (d, J = 7.9 Hz, 1H), 7.33 (dt, J = 8.1, 0.8 Hz, 1H), 7.25 (m, 2H), 7.14 (dd, J = 8.2, 1.6 Hz, 1H), 7.06 (m, 2H), 6.93 (m, 1H), 3.67 (s, 2H). ^{13}C NMR (101 MHz, DMSO, δ = ppm): 170.16, 153.03, 143.46, 139.53, 138.03, 137.06, 136.55, 134.34, 132.25, 131.93, 129.42, 127.88, 127.63, 126.30, 124.84, 124.58, 123.64 (d, J = 6.2 Hz), 123.09, 121.49, 118.98, 118.89, 111.81, 108.27, 33.77. Anal. calcd. for $\text{C}_{25}\text{H}_{19}\text{N}_3\text{O}_4\text{S}$: C, 65.63; H, 4.19; N, 9.18; S, 7.01%. Found: C, 65.57; H, 4.24; N, 9.39; S, 7.25%.

2-(2-(1H-indol-3-yl)acetamido)phenyl thiophene-2-sulfonate (5n). Yield: 82.01%, R_f = 0.4, (*n*-hexane/ethyl acetate = 1 : 4), colour: off-white solid, mp: 180–183 °C, FT-IR ($\bar{\nu}$, cm^{-1}): 3431 (N–H, stretching), 2925 (C–H, stretching), 1649 (C=O, stretching), 1083 (S=O, stretching); ^1H NMR (400 MHz, DMSO, δ = ppm): 10.96 (s, 1H), 9.42 (s, 1H), 8.06 (d, J = 5.0 Hz, 1H), 7.83 (d, J = 8.1 Hz, 1H), 7.56 (d, J = 8.1 Hz, 2H), 7.36 (d, J = 8.1 Hz, 1H), 7.29–7.18 (m, 3H), 7.17–7.03 (m, 3H), 6.99 (t, J = 7.6 Hz, 1H), 3.66 (s, 2H). ^{13}C NMR (101 MHz, DMSO, δ = ppm): 170.01, 140.20, 137.76, 136.75, 136.57, 133.40, 131.72, 128.80, 128.15, 127.75, 125.05, 124.61, 124.37, 123.13, 121.51, 119.25, 118.90, 111.83, 108.61, 33.50. Anal. calcd. for $\text{C}_{20}\text{H}_{16}\text{N}_2\text{O}_4\text{S}_2$: C, 58.24; H, 3.91; N, 6.79; S, 15.55%. Found: C, 58.31; H, 3.84; N, 6.70; S, 15.58%.

2-(2-(1H-indol-3-yl)acetamido)phenyl 4-methylbenzenesulfonate (5o). Yield: 78.61%, R_f = 0.5, (*n*-hexane/ethyl acetate = 1 :



4), colour: white solid, mp: 160–162 °C, FT-IR ($\bar{\nu}$, cm^{-1}): 3404 (N–H, stretching), 2955 (C–H, stretching), 1519 (C=O, stretching), 1373 (S=O, stretching); ^1H NMR (400 MHz, DMSO, δ = ppm): 10.95 (s, 1H), 9.47 (s, 1H), 7.77 (m, 2H), 7.53 (dd = 8.06, 1.71 Hz, 2H), 7.42 (d = 8.11 Hz, 1H), 7.36 (d = 8.07 Hz, 1H), 7.26 (m, 3H), 7.15 (td = 7.79, 1.69 Hz, 1H), 7.08 (m, 1H), 6.98 (m, 1H), 3.58 (s, 2H), 2.35 (s, 3H). ^{13}C NMR (101 MHz, DMSO, δ = ppm): 169.91, 140.63, 140.15, 136.55, 133.39, 131.43, 130.50, 130.16, 128.14, 127.72, 125.26, 124.70, 124.53, 123.25, 121.54, 119.21, 118.92, 111.86, 108.56, 33.37, 20.36. Anal. calcd. for $\text{C}_{23}\text{H}_{20}\text{N}_2\text{O}_4\text{S}$: C, 65.70; H, 4.79; N, 6.66; S, 7.62%. Found: C, 65.53; H, 4.84; N, 6.72; S, 7.55%.

Enzyme inhibition assays

Transfection. COS-7 cells were transfected with plasmids encoding Human (*h*) ENPP1 (GenBank accession no. NM_006208, a kind gift of James W. Goding, *h*-ENPP3 (GenBank accession no. NM_005021),^{72,73} a kind gift of Kimihiko Sano, *h*-e5'NT (GenBank accession no. DQ186653),⁷⁴ *r*-e5'NT (GenBank accession no. NM_021576),⁷⁵ a kind gift of Herbert Zimmermann, and *h*-TNAP (GenBank accession no. NM_000478) a kind gift from Professor José Luis Millan.⁷⁶ Each plasmid DNA sample (6 μg), and 24 μL of lipofectamine reagent were added to a 10 cm dish plate directly in the medium and then incubated at 37 °C for 5 hours in DMEM/F-12 without fetal bovine serum. The transfection process was stopped by the addition of an equal volume of DMEM/F-12 supplemented with 20% fetal bovine serum (FBS). Transfected cells were extracted as described earlier⁷⁷ after 48–72 hours.

Membrane fractions preparation. At 4 °C, Tris-saline was used to wash the transfected COS-7 cells. For scraping cells, a harvesting buffer containing 95 mM NaCl, 0.1 mM PMSF, and 45 mM Tris at pH 7.5 was utilized. The scraped cells were centrifuged twice (300 g each time), for 5 min. each, at 4 °C.⁷⁷ The harvesting buffer was amended with aprotinin (10 μg mL^{-1}), and the cells were then resuspended and sonicated. To separate the nuclear and cell debris, centrifugation at 850g for 5 min at 4 °C was once more performed. The obtained supernatant was mixed with 7.5% glycerol and kept at –80 °C. The protein concentration was calculated using the Bradford microplate test, using bovine serum albumin as the reference protein.⁷⁸

***h*-ENPP1 and *h*-ENPP3 assay.** The inhibitory action of newly synthesized compounds was measured using a method previously reported with little modifications.⁷⁹ The assay buffer had a final pH of 9.5 and contained 50 mM Tris. HCl, 5 mM MgCl_2 , and 0.1 mM ZnCl_2 . The synthesized compounds for screening against *h*-ENPPs were prepared in 10% DMSO and tested at 0.1 mM concentration in assay. The assay was performed in 96-well plate keeping total assay volume 100 μL per well which contain assay buffer, 100 μM of test compound, enzymes *h*-ENPP1 (27 ng), *h*-ENPP3 (35 ng) and substrate *p*-nitrophenyl 5'-thymidine monophosphate. After 25 minutes in the incubator at 37 °C, absorbance was measured at 405 nm with a microplate reader (BIOTEK ELX800™, Instruments, Inc., USA). The compounds that showed more than 50% inhibition of either *h*-

ENPP1 or *h*-ENPP3 were subjected to serial dilutions for the determination of IC_{50} values. The data was analyzed by using non-linear regression analysis curve fitting program PRISM 5.0 (Graph Pad, San Diego, California, USA).

CD73 (*h*-e5'NT, *r*-e5'NT) assay. The e5'NT inhibition assays were carried out on both human and rat enzymes as previously described.⁸⁰ Tris HCl (10 mM), MgCl_2 , and CaCl_2 were the components of the test buffer, and the pH was raised to 7.4 before use. To check whether the compounds had any activity, the assay was initially run in triplicate. The assay's overall volume was 100 μL . Each well received 55 μL of the assay buffer in triplicate, followed by 10 μL of the e5'NT. A total of 10 μL of test compounds with a final concentration of 100 mM were added to each well. The incubation period was 10 minutes at 37 °C. After adding 10 μL of AMP (2 mM) as a substrate, the enzymatic reaction commenced and kept going for 20 minutes at 37 °C. The amount of phosphate released during the enzyme-mediated breakdown of the substrate was then determined by adding 15 μL of malachite green reagent, and the change in absorbance at 630 nm was measured. The test substances were employed in varied concentrations to determine the IC_{50} values using the same approach. GraphPad Prism® 5.0 software (San Diego, CA, USA) used the nonlinear regression analysis method to further analyze the IC_{50} values of only those compounds that had an inhibition value greater than 50%.

***h*-TNAP assay.** The effects of recently synthesized substances on human tissue non-specific alkaline phosphatase (*h*-TNAP) were evaluated. Using the previously mentioned procedure,⁸¹ the compounds were first evaluated against *h*-TNAP enzymes at a concentration of 1 mM. Glycerol made up half of the assay buffer (pH 9.5), which also contained Tris-hydrochloride (50 mM), MgCl_2 (5 mM), and ZnCl_2 (0.1 mM) in the solution. Tris-hydrochloride (50 mM), MgCl_2 , and ZnCl_2 (0.1 mM) made up the dilution buffer. By using a dilution buffer, the enzyme, substrate *p*-nitrophenyl phosphate (*p*-NPP), and all requisite test chemicals were diluted to the appropriate concentration. The absorbance of the released *p*-nitrophenolate was measured after a second incubation at 405 nm employing a 96-well microplate reader (BIOTEK ELX 800™, Instruments, Inc., USA). Calculations were made to determine the percentage inhibition of the standard (levamisole) and the other drugs. Following the same process used in initial screening, three times in triplicate, the compounds with more than 50% inhibition were chosen for further IC_{50} values determination. GraphPad Prism 5.0 software (San Diego, California, USA) was used to determine the IC_{50} values of the molecules showing greater than 50% inhibition at 100 μM .

Enzyme kinetics studies

The enzyme kinetic research was carried out utilizing a series of substrate concentrations of 0, 1.25, 2.5, 5.0, 7.5, and 10 mM. For most potent inhibitors **5c**, **5e**, **5g**, **5i** and **5j** concentrations utilized were based on the IC_{50} values from *in vitro* assays with two concentrations above and two below the determined IC_{50} value concentrations. The test plate was made by adding the enzyme per well (*in vitro* assay concentration of respective



enzyme assays afore mentioned) to the assay buffer. A microplate reader (BIOTEK ELX800™, Instruments, Inc., USA) was used to record the reading after the assay mixture had been incubated at 37 °C for 25 minutes. Lineweaver–Burk graphs with PRISM 5.0 (Graph Pad, San Diego, California, USA) was used to analyze the data.

Molecular docking

The Molecular Operating Environment software (MOE) 2019.0102 (ref. 82) was employed to perform molecular docking studies on the synthesized derivatives (5a–5o). The docking studies was carried out by using the Protein data Bank <https://www.rcsb.org/> under PDB ID 6WEW and 4H2G for human ectonucleotide pyrophosphatase/phosphodiesterase 1 (*h*-ENPP1) and *h*-e5'NT while homology models were used for *r*-e5'NT, *h*-ENPP3 and *h*-TNAP. Standard inhibitors were docked along with synthesized ligands to validate the docking results. *N*-(4-[(7-methoxyquinolin-4-yl)oxy]phenyl)sulfuric diamide (TZV) a co-crystal was used as standard for both human *h*-ENPP1 and *h*-ENPP3. Suramin was taken as standard inhibitor for human and rat ecto-5'-nucleotidase and in case of *h*-TNAP, levamisole was considered as standard inhibitor.

Chemical structures were sketched using chemDraw Ultra 12.0 and energy was minimized using MMFF-94 force field implemented in MOE.⁸³ The addition of hydrogen atoms was carried out to the model structure and then ionization states of metals ions were prepared to be fixed. Docking was performed by using the refinement features where induced fit receptor and triangular matcher was selected. The best pose was selected which exhibited top-ranked minimum binding energy and RMSD value less than 2.⁸⁴ The re-docking of the identified derivatives was carried out for the validation of the docking results.

Author contributions

Muhammad Siraj Khan Jadoon: conceptualization, synthesis, characterization, methodology, formal analysis, validation investigation (bioactivity), docking studies, writing – original draft preparation, software. Julie Pelletier, Jean Sévigny: expression of recombinant enzymes. Jamshed Iqbal: supervision, resources (synthesis), data curation, writing – original draft reviewing and editing, supervision, resources (bioactivity and docking), funding acquisition.

Conflicts of interest

The authors declare that they have no significant conflict of interest.

Acknowledgements

The authors gratefully acknowledge the financial support for this research provided by the Higher Education Commission of Pakistan (HEC) via NRP project no. 20-15846/NRP/R&D/HEC/2021-2020, German–Pakistani Research Collaboration Program and Equipment Grant funded by DAAD, Germany. J. S. received

support from the Natural Sciences and Engineering Research Council of Canada (RGPIN-2023-05498).

References

- 1 J. Candido and T. Hagemann, Cancer-related inflammation, *J. Clin. Immunol.*, 2013, **33**, 79–84.
- 2 A. Kalbasi and A. Ribas, Tumour-intrinsic resistance to immune checkpoint blockade, *Nat. Rev. Immunol.*, 2020, **20**(1), 25–39.
- 3 D. Bedognetti, *et al.*, Toward a comprehensive view of cancer immune responsiveness: a synopsis from the SITC workshop, *J. Immunother. Cancer*, 2019, **7**(1), 1–23.
- 4 P. Sharma and J. P. Allison, Immune checkpoint targeting in cancer therapy: toward combination strategies with curative potential, *Cell*, 2015, **161**(2), 205–214.
- 5 J. Stagg and M. Smyth, Extracellular adenosine triphosphate and adenosine in cancer, *Oncogene*, 2010, **29**(39), 5346–5358.
- 6 L.-l. Feng, *et al.*, The yin and yang functions of extracellular ATP and adenosine in tumor immunity, *Cancer Cell Int.*, 2020, **20**(1), 1–11.
- 7 H. Zimmermann, 5'-Nucleotidase: molecular structure and functional aspects, *Biochem. J.*, 1992, **285**(Pt 2), 345.
- 8 L. Antonioli, *et al.*, CD39 and CD73 in immunity and inflammation, *Trends Mol. Med.*, 2013, **19**(6), 355–367.
- 9 N. Sträter, Ecto-5'-nucleotidase: Structure function relationships, *Purinergic Signal.*, 2006, **2**(2), 343.
- 10 D. Allard, *et al.*, Targeting the CD73-adenosine axis in immuno-oncology, *Immunol. Lett.*, 2019, **205**, 31–39.
- 11 J. L. Millán, Alkaline phosphatases: structure, substrate specificity and functional relatedness to other members of a large superfamily of enzymes, *Purinergic Signal.*, 2006, **2**, 335–341.
- 12 M. Picher, *et al.*, Ecto 5'-nucleotidase and nonspecific alkaline phosphatase: two AMP-hydrolyzing ectoenzymes with distinct roles in human airways, *J. Biol. Chem.*, 2003, **278**(15), 13468–13479.
- 13 M. al-Rashida and J. Iqbal, Therapeutic potentials of ecto-nucleoside triphosphate diphosphohydrolase, ecto-nucleotide pyrophosphatase/phosphodiesterase, ecto-5'-nucleotidase, and alkaline phosphatase inhibitors, *Med. Res. Rev.*, 2014, **34**(4), 703–743.
- 14 D. Vijayan, *et al.*, Targeting immunosuppressive adenosine in cancer, *Nat. Rev. Cancer*, 2017, **17**(12), 709–724.
- 15 S. C. Robson, J. Sévigny and H. Zimmermann, The E-NTPDase family of ectonucleotidases: structure function relationships and pathophysiological significance, *Purinergic Signal.*, 2006, **2**, 409–430.
- 16 J. B. Volmer, L. F. Thompson and M. R. Blackburn, Ecto-5'-nucleotidase (CD73)-mediated adenosine production is tissue protective in a model of bleomycin-induced lung injury, *J. Immunol.*, 2006, **176**(7), 4449–4458.
- 17 M. R. C. Schetinger, *et al.*, NTPDase and 5'-nucleotidase activities in physiological and disease conditions: New perspectives for human health, *Biofactors*, 2007, **31**(2), 77–98.



- 18 A. El-Tayeb, *et al.*, Nucleoside-5'-monophosphates as prodrugs of adenosine A2A receptor agonists activated by ecto-5'-nucleotidase, *J. Med. Chem.*, 2009, **52**(23), 7669–7677.
- 19 B. B. Fredholm, *et al.*, International Union of Basic and Clinical Pharmacology. LXXXI. Nomenclature and classification of adenosine receptors—an update, *Pharmacol. Rev.*, 2011, **63**(1), 1–34.
- 20 S. Ryzhov, *et al.*, Adenosinergic regulation of the expansion and immunosuppressive activity of CD11b+ Gr1+ cells, *J. Immunol.*, 2011, **187**(11), 6120–6129.
- 21 A. Buffon, *et al.*, Differential expression of nucleotide pyrophosphatase/phosphodiesterases by Walker 256 mammary cancer cells in solid tumors and malignant ascites, *Life Sci.*, 2010, **86**(11–12), 435–440.
- 22 N. A. Sowa, M. K. Voss and M. J. Zylka, Recombinant ecto-5'-nucleotidase (CD73) has long lasting antinociceptive effects that are dependent on adenosine A1 receptor activation, *Mol. Pain*, 2010, **6**, 20.
- 23 I. D. Goldfine, *et al.*, The role of membrane glycoprotein plasma cell antigen 1/ectonucleotide pyrophosphatase phosphodiesterase 1 in the pathogenesis of insulin resistance and related abnormalities, *Endocr. Rev.*, 2008, **29**(1), 62–75.
- 24 L. Bavaresco, *et al.*, The role of ecto-5'-nucleotidase/CD73 in glioma cell line proliferation, *Mol. Cell. Biochem.*, 2008, **319**, 61–68.
- 25 J. Stella, *et al.*, Differential ectonucleotidase expression in human bladder cancer cell lines, in *Urologic Oncology: Seminars and Original Investigations*, Elsevier, 2010.
- 26 J. Szychala, *et al.*, Role of estrogen receptor in the regulation of ecto-5'-nucleotidase and adenosine in breast cancer, *Clin. Cancer Res.*, 2004, **10**(2), 708–717.
- 27 L. Antonioli, *et al.*, Switching off CD73: a way to boost the activity of conventional and targeted antineoplastic therapies, *Drug Discovery Today*, 2017, **22**(11), 1686–1696.
- 28 I. Perrot, *et al.*, Blocking antibodies targeting the CD39/CD73 immunosuppressive pathway unleash immune responses in combination cancer therapies, *Cell Rep.*, 2019, **27**(8), 2411–2425.
- 29 N. Sträter, Ecto-5'-nucleotidase: Structure function relationships, *Purinergic Signal.*, 2006, **2**, 343–350.
- 30 R. Sadej, J. Szychala and A. C. Skladanowski, Expression of ecto-5'-nucleotidase (eN, CD73) in cell lines from various stages of human melanoma, *Melanoma Res.*, 2006, **16**(3), 213–222.
- 31 R. Resta, Y. Yamashita and L. F. Thompson, Ecto-enzyme and signaling functions of lymphocyte CD 7 3, *Immunol. Rev.*, 1998, **161**(1), 95–109.
- 32 J. Szychala, Tumor-promoting functions of adenosine, *Pharmacol. Ther.*, 2000, **87**(2–3), 161–173.
- 33 F. Gendron, *et al.*, Purine signaling and potential new therapeutic approach: possible outcomes of NTPDase inhibition, *Curr. Drug Targets*, 2002, **3**(3), 229–245.
- 34 J. Iqbal, *et al.*, A highly sensitive CE-UV method with dynamic coating of silica-fused capillaries for monitoring of nucleotide pyrophosphatase/phosphodiesterase reactions, *Electrophoresis*, 2008, **29**(17), 3685–3693.
- 35 A. Tokumura, *et al.*, Identification of human plasma lysophospholipase D, a lysophosphatidic acid-producing enzyme, as autotaxin, a multifunctional phosphodiesterase, *J. Biol. Chem.*, 2002, **277**(42), 39436–39442.
- 36 H.-J. Bühring, A. Streble and P. Valent, The basophil-specific ectoenzyme E-NPP3 (CD203c) as a marker for cell activation and allergy diagnosis, *Int. Arch. Allergy Appl. Immunol.*, 2004, **133**(4), 317–329.
- 37 C. Stefan, S. Jansen and M. Bollen, Modulation of purinergic signaling by NPP-type ectophosphodiesterases, *Purinergic Signal.*, 2006, **2**, 361–370.
- 38 B. Grobbsen, P. De Deyn and H. Slegers, Rat C6 glioma as experimental model system for the study of glioblastoma growth and invasion, *Cell Tissue Res.*, 2002, **310**, 257–270.
- 39 I. Aerts, *et al.*, The expression of ecto-nucleotide pyrophosphatase/phosphodiesterase 1 (E-NPP1) is correlated with astrocytic tumor grade, *Clin. Neurol. Neurosurg.*, 2011, **113**(3), 224–229.
- 40 N. Ruf, *et al.*, The mutational spectrum of ENPP1 as arising after the analysis of 23 unrelated patients with generalized arterial calcification of infancy (GACI), *Hum. Mutat.*, 2005, **25**(1), 98.
- 41 M.-L. He, *et al.*, Release and extracellular metabolism of ATP by ecto-nucleotidase eNTPDase 1–2 in hypothalamic and pituitary cells, *Purinergic Signalling*, 2005, **1**, 135–144.
- 42 U. Sharma, D. Pal and R. Prasad, A novel role of alkaline phosphatase in the ERK1/2 dephosphorylation in renal cell carcinoma cell lines: a new plausible therapeutic target, *Biochimie*, 2014, **107**, 406–409.
- 43 A. Kozlenkov, *et al.*, Residues determining the binding specificity of uncompetitive inhibitors to tissue-nonspecific alkaline phosphatase, *J. Bone Miner. Res.*, 2004, **19**(11), 1862–1872.
- 44 J. M. Kim, *et al.*, The effect of alkaline phosphatase and intrahepatic metastases in large hepatocellular carcinoma, *World J. Surg. Oncol.*, 2013, **11**, 1–8.
- 45 I. Ali, *et al.*, Heterocyclic scaffolds: centrality in anticancer drug development, *Curr. Drug Targets*, 2015, **16**(7), 711–734.
- 46 S. S. Gholap, Pyrrole: An emerging scaffold for construction of valuable therapeutic agents, *Eur. J. Med. Chem.*, 2016, **110**, 13–31.
- 47 S. Ahmad, *et al.*, Pyrrole: An insight into recent pharmacological advances with structure activity relationship, *Eur. J. Med. Chem.*, 2018, **157**, 527–561.
- 48 M. A. Tantawy, *et al.*, Auspicious role of the steroidal heterocyclic derivatives as a platform for anti-cancer drugs, *Bioorg. Chem.*, 2017, **73**, 128–146.
- 49 G. M. das Neves, *et al.*, Targeting ecto-5'-nucleotidase: A comprehensive review into small molecule inhibitors and expression modulators, *Eur. J. Med. Chem.*, 2023, **247**, 115052.
- 50 J. L. Jeffrey, K. V. Lawson and J. P. Powers, Targeting metabolism of extracellular nucleotides via inhibition of ectonucleotidases CD73 and CD39, *J. Med. Chem.*, 2020, **63**(22), 13444–13465.
- 51 L. Schäkel, *et al.*, Nucleotide analog ARL67156 as a lead structure for the development of CD39 and dual CD39/



- CD73 ectonucleotidase inhibitors, *Front. Pharmacol.*, 2020, **11**, 1294.
- 52 K. V. Lawson, *et al.*, Discovery of AB680: a potent and selective inhibitor of CD73, *J. Med. Chem.*, 2020, **63**(20), 11448–11468.
- 53 M. I. Choudhary, *et al.*, New biscoumarin derivatives-cytotoxicity and enzyme inhibitory activities, *Bioorg. Med. Chem.*, 2006, **14**(23), 8066–8072.
- 54 Y. Baqi, *et al.*, Development of potent and selective inhibitors of ecto-5'-nucleotidase based on an anthraquinone scaffold, *J. Med. Chem.*, 2010, **53**(5), 2076–2086.
- 55 P. Frasson Corbelini, *et al.*, Insights into Ecto-5'-nucleotidase as a new target for cancer therapy: a medicinal chemistry study, *Curr. Med. Chem.*, 2015, **22**(15), 1776–1792.
- 56 R. B. Giordani, *et al.*, Trichomonas vaginalis nucleoside triphosphate diphosphohydrolase and ecto-5'-nucleotidase activities are inhibited by lycorine and candimine, *Parasitol. Int.*, 2010, **59**(2), 226–231.
- 57 A. Fiene, *et al.*, Inhibitors for the bacterial ectonucleotidase Lp1NTPDase from Legionella pneumophila, *Bioorg. Med. Chem.*, 2016, **24**(18), 4363–4371.
- 58 S. Ullah, *et al.*, Synthesis and Biological Evaluation of Arylamide Sulphonate Derivatives as Ectonucleotide Pyrophosphatase/Phosphodiesterase-1 and-3 Inhibitors, *ACS Omega*, 2022, **7**(30), 26905–26918.
- 59 H. Ahmad, *et al.*, Synthesis of biphenyl oxazole derivatives via Suzuki coupling and biological evaluations as nucleotide pyrophosphatase/phosphodiesterase-1 and-3 inhibitors, *Eur. J. Med. Chem.*, 2020, **208**, 112759.
- 60 M. I. El-Gamal, *et al.*, Synthesis, biological evaluation, and docking studies of new raloxifene sulfonate or sulfamate derivatives as inhibitors of nucleotide pyrophosphatase/phosphodiesterase, *Eur. J. Med. Chem.*, 2019, **181**, 111560.
- 61 A. I. Shahin, *et al.*, Design and synthesis of new adamantyl derivatives as promising antiproliferative agents, *Eur. J. Med. Chem.*, 2023, **246**, 114958.
- 62 M. Lind, Principles of systemic anticancer therapy, *Medicine*, 2020, **48**(2), 90–96.
- 63 L. Cyr, *et al.*, Antiproliferative effects of a series of novel synthetic sulfonate esters on human breast cancer cell line MCF-7, *Anticancer Res.*, 2007, **27**(3B), 1437–1448.
- 64 S. Ullah, *et al.*, Synthesis, biological evaluation, and docking studies of new pyrazole-based thiourea and sulfonamide derivatives as inhibitors of nucleotide pyrophosphatase/phosphodiesterase, *Bioorg. Chem.*, 2020, **99**, 103783.
- 65 E. Mahmoud, *et al.*, Recent progress in biologically active indole hybrids: A mini review, *Pharmacol. Rep.*, 2022, **74**(4), 570–582.
- 66 D. Kumar, *et al.*, Synthesis and identification of α -cyano bis (indolyl) chalcones as novel anticancer agents, *Bioorganic Med. Chem. Lett.*, 2014, **24**(22), 5170–5174.
- 67 A. J. Yee and N. S. Raje, Panobinostat and multiple myeloma in 2018, *Oncologist*, 2018, **23**(5), 516–517.
- 68 S. Peters, *et al.*, Alectinib versus crizotinib in untreated ALK-positive non-small-cell lung cancer, *N. Engl. J. Med.*, 2017, **377**(9), 829–838.
- 69 R. J. Motzer, *et al.*, Sunitinib in patients with metastatic renal cell carcinoma, *JAMA*, 2006, **295**(21), 2516–2524.
- 70 J.-C. Soria, *et al.*, Osimertinib in untreated EGFR-mutated advanced non-small-cell lung cancer, *N. Engl. J. Med.*, 2018, **378**(2), 113–125.
- 71 G. J. Roth, *et al.*, Nintedanib: from discovery to the clinic, *J. Med. Chem.*, 2015, **58**(3), 1053–1063.
- 72 S. I. Belli and J. W. Goding, Biochemical characterization of human PC-1, an enzyme possessing alkaline phosphodiesterase I and nucleotide pyrophosphatase activities, *Eur. J. Biochem.*, 1994, **226**(2), 433–443.
- 73 P. Jin-Hua, *et al.*, Molecular cloning and chromosomal localization of PD-I β (PDNP3), a new member of the human phosphodiesterase I genes, *Genomics*, 1997, **45**(2), 412–415.
- 74 J. Lecka, M. S. Rana and J. Sévigny, Inhibition of vascular ectonucleotidase activities by the pro-drugs ticlopidine and clopidogrel favours platelet aggregation, *Br. J. Pharmacol.*, 2010, **161**(5), 1150–1160.
- 75 Y. Misumi, *et al.*, Primary structure of rat liver 5'-nucleotidase deduced from the cDNA. Presence of the COOH-terminal hydrophobic domain for possible post-translational modification by glycopospholipid, *J. Biol. Chem.*, 1990, **265**(4), 2178–2183.
- 76 T. Kiffer-Moreira, *et al.*, Catalytic signature of a heat-stable, chimeric human alkaline phosphatase with therapeutic potential, *PLoS One*, 2014, **9**(2), e89374.
- 77 S. Lévesque, *et al.*, Specificity of the ecto-ATPase inhibitor ARL 67156 on human and mouse ectonucleotidases, *Br. J. Pharmacol.*, 2007, **152**(1), 141–150.
- 78 M. M. Bradford, A rapid and sensitive method for the quantitation of microgram quantities of protein utilizing the principle of protein-dye binding, *Anal. Biochem.*, 1976, **72**(1–2), 248–254.
- 79 S. Ullah, *et al.*, Synthesis, biological evaluation, and docking studies of novel pyrrolo [2, 3-*b*] pyridine derivatives as both ectonucleotide pyrophosphatase/phosphodiesterase inhibitors and antiproliferative agents, *Eur. J. Med. Chem.*, 2021, **217**, 113339.
- 80 M. Adzic and N. Nedeljkovic, Unveiling the role of ecto-5'-nucleotidase/CD73 in astrocyte migration by using pharmacological tools, *Front. Pharmacol.*, 2018, **9**, 153.
- 81 I. Khan, *et al.*, Influence of the diversified structural variations at the imine functionality of 4-bromophenylacetic acid derived hydrazones on alkaline phosphatase inhibition: synthesis and molecular modelling studies, *RSC Adv.*, 2015, **5**(110), 90806–90818.
- 82 Molecular Operating Environment (MOE), *Chemical Computing Group ULC*, 1010 Sherbrooke St. West, Suite #910, Montreal, AC, Canada, H3A 2R7, 2020.
- 83 L. Heinzerling, R. Klein and M. Rarey, Fast force field-based optimization of protein–ligand complexes with graphics processor, *J. Comput. Chem.*, 2012, **33**(32), 2554–2565.
- 84 Z. Wang, *et al.*, Comprehensive evaluation of ten docking programs on a diverse set of protein–ligand complexes: the prediction accuracy of sampling power and scoring power, *Phys. Chem. Chem. Phys.*, 2016, **18**(18), 12964–12975.

